Forum geografic. Studii și cercetări de geografie și protecția mediului
Volume **XXIII**, Issue **1** (**June 2024**), pp. **16-43;** DOI: **10.5775/fg.2024.1.3629**

Mapping desertification susceptibility in the Hodna watershed Algeria, using a remote sensing-based logistic regression approach

Takki Eddine KHARCHI[1,*], Mohammed CHADI[1], Chaouki BENABBAS[2], Florina GRECU[3], Manel YEKHLEFOUNE[1]

[1] Department of Urban Techniques and Environment, Institute of Urban Techniques Management, University of Constantine 3, Geo-prospective, Environment, and Development Laboratory, Constantine, Algeria
[2] Centre de Recherche en Aménagement du Territoire (CRAT), Campus Zouaghi Slimane, Route de Ain el Bey, 25000 Constantine, Algérie
[3] Department of Geomorphology, Pedology, Geomatics, Faculty of Geography, University of Bucharest, Bucharest, Romania
* *Corresponding author*: takkieddine.kharchi@univ-constantine3.dz

Received on 08-12-2023, reviewed on 22-05-2024, accepted on 28-06-2024

Abstract

This study aims to identify regions prone to desertification in the Hodna basin, which covers a vast area of the vulnerable Algerian Steppes. Thirteen factors were selected as independent variables: geomorphological factors (wind and water erosion, Topographic Position Index (TPI), Drainage Density, Slope, Aspect, Elevation), environmental factors (Normalized Difference Vegetation Index (NDVI) and Evapotranspiration), soil factors (Land surface Temperature (LST) and Normalized Difference Salinity Index (NDSI), and socio-economic factors (the Human Influence Index (HII) and the Livestock. Due to the lack of previous desertification data, NDVI anomalies served as the dependent variable. all of the variables were mainly derived using remote sensing techniques and a logistic regression model was applied for analysis in the R environment for desertification susceptibility mapping, displaying stable predictive power with a Receiver Operating Characteristic (ROC) curve of 0.76. Unlike the Northern part of the Mediterranean, where water erosion is predominant, wind erosion and soil salinization emerged as key factors in this study, while the socio-economic factors had less influence than anticipated. The resulting map shows that 45.4% of the basin is highly to very highly susceptible to desertification, provinding essential data for targeted intervention strategies.
Keywords: *Hodna watershed, logistic regression, desertification, erosion, susceptibility mapping*

Introduction

Desertification is a global environmental concern described as the land degradation in drylands that encompasses arid, semi-arid and dry sub-humid areas caused by extreme hydro-climatic events, that complex interaction and concomitance of these events with several factors including climatic fluctuations and human actions increase their frequency and intensity (Yakhlefoune et al., 2023) moreover the United Nations Convention to Combat Desertification (UNCCD) identifies land degradation as a reduction or loss of the biological or economic productivity and complexity of land use and land cover in these regions resulting from a combination of processes including those originating from human activities and settlement patterns like soil erosion caused by wind or water; deterioration of the physical, chemical, biological or the economic proprieties of soil and long-term loss of vegetation cover (Parry, 2007; Borsali et al., 2019). In addition, based on the Contribution of the Working Group II to the Sixth Assessment Report of the Intergovernmental Panel on Climate Change (IPCC) (Mirzabaev et al., 2022) there is substantial evidence of the existence of desertification in deserts therefore we can include the hyper-arid areas to the definition of the desertification phenomenon.

Algeria is one of the most threatened countries by desertification in Northern Africa and the Mediterranean region, of its total surface of 230 million hectares 84% is unaltered deserts while 5% are mountainous areas prone to water erosion while 8.4% are steppic areas and 35% of it is highly sensitive to desertification (Merdas et al., 2019), Considering the major role they play in the country's agricultural economy they are subject to anthropogenic pressure like overgrazing, inappropriate land use management and severe drought events due to climate change (Kouba et al., 2021) they are the most vulnerable areas to the land degradation and desertification phenomenon (Bouhata & Kalla, 2014). Moreover, the importance of studying the Hodna watershed lies in the fact that it encompasses a vast area of the steppe regions, these areas are comprised between the Atlas mountains within the Atlas Tellian North and the Atlas Saharan South making a natural barrier against the progression of the desert towards the North (Benazzouz & Boureboune, 2009).

Several methods, mapping and assessment techniques have emerged during the last decadic periods used for the study and evaluation of desertification, essentially remote sensing based approaches were used namely change detection and bi-temporal change detection methods such as spectral mixture analysis (SMA); linear mixture model (LMM); change vector analysis (CVA); principal component analysis (PCA); iterative principal component analysis (IPCA); multivariate alteration detection (MAD), image differencing, long-term study of NDVI and rainfall, supervised classification methods and multi-criteria evaluation (Albalawi & Kumar, 2013). There are few limitations associated with these techniques which let alone does not provide sufficient data to draw a compelling conclusion (Albalawi & Kumar, 2013) due to spatial resolution issues and scales, the quality and availability of data, the absence of consistency across different studies making it a difficult task to analogize and integrate results, the complexity of desertification and its temporal dynamics, inadequacies in capturing human interactions and the socioeconomic factors and finally the limitations of ground-truth validation.

Other than that, Kosmas et al. (1999) proposed a holistic approach to better capture human-environment interactions. The Mediterranean Desertification and Land Use (MEDALUS) model, which was later updated by Ferrara et al. (2020), incorporates both natural and human factors contributing to desertification. This model has proven effective and is widely used across several Mediterranean regions, yet its limitation lies in the fact that it was designed for the northern Mediterranean environments where water erosion is the primary issue unlike arid regions where the main concerns are wind erosion and soil salinization (Kosmas et al., 1999), a concern emphasized also by (Gad, 2020) and may necessitate adjustments like the study of (Boudjemline & Semar, 2018) for example applied to the Hodna Watershed. In the light of that and seeking a method that allows more freedom and flexibility in choosing and including variables we applied the logistic regression method, a widely recognized and accepted approach in so many fields, for instance in geoscience, especially for hazards it has been applied for landslide studies (Brenning, 2005), flood susceptibility modelling (Mind'je et al., 2019), earthquake to perform seismic vulnerability assessment (Han et al., 2019), erosion (Conoscenti et al., 2014), volcanic hazard activity (Junek et al., 2012) and desertification (Djeddaoui et al., 2017; Mihi et al., 2022).

The primary goal of our study is identifying and mapping desertification susceptibility in the Hodna watershed which occupies a vast region of the Algerian steppe considered highly vulnerable to desertification with serious consequences on the local economy including important factors such as erosion and soil salinization to then carry out a reliability and stability assessment of the predictive model applying the Receiver Operating Characteristics (ROC), goodness of fit and the multicollinearity diagnosis. Providing key elements and an up-to-date susceptibility map of desertification that helps in the decision-making process to take appropriate precautionary actions to combat and mitigate desertification.

Study Area

The Hodna watershed is one of the basins of the Algerois-Hodna-Soummam hydrographic region it is situated between latitudes 34°N & 36°N and longitudes 3°E & 6°E. According to the National Agency of Integrated Water Resources Management in Algeria (AGIRE), the Hodna is an endoreic basin it covers a considerable area of 25843 km² representing 54% of the total area of the Hydrographic basin of the Algerois-Hodna-Soummam and draining into a closed depression of Chott El Hodna at 400 meters of altitude , it is surrounded North by the Isser and Soummam watersheds being part of the same hydrographic region, West by the Chellif-Zahrez basin, East by the Constantinois-Seybousse-Méllague basin and South by the Saharan region. It represents the transition between the Atlas Tellian chain highlighted by the East-West Hodna mountains with the culminant peak of mountain Tacherift Guetiane at 1900 meters East tapering towards the West down to 1000 meters and South the Saharan Atlas chain forming a barrier not transcending 1200 meters. The basin spans over 7 districts counting parts of Médea, Bouira, Sétif, Bordj Bou Arreridj, Batna, M'sila et Djelfa and the population census exceeded 2 million in 2014 comprising 100 municipalities and 259 agglomerations.

In accordance with the climatic classification of Gaussen (1937) most of the hydrometric stations of the basin show a dry arid climate except for the station of Bordj Bou Arreridj in the Northmost presenting Mediterranean climate (Kebiche, 1994), a Mediterranean climate with arid tendencies mainly due to the Saharan influence with mean annual precipitation of more than 800 mm for the Atlas Tellian relief, around 200 to 400 mm for the high steppe plains considered the transition between the Atlas mountains chain and less than 100 mm for the Southern borders of the Atlas Saharan and the depression of Chott El Hodna while high altitudes of the Atlas Saharan receives a considerable amount of precipitation like for instance Ain Oghrab at 1304 meters with 323.5 mm, moreover the thermal regime which has a strong correlation with precipitation displays substantial fluctuations ranging from (-0.6°) in winter to around (40°) in summer (Kaabeche, 1996).

The primary geological and geomorphological traits of the basin are an alternation of clayey marls and limestone levels back to the Cenomanian period composing the relief, flat surfaces formed by alluvial deposits from the quaternary representing the Glacis (chebket), depressions which are zones of concentration of runoff water and sedimentation of solid particles classified into two categories salty nature (Sebkha, Chott) and non-salty nature (Daya) and finally dunes, heaps of quartz sands rich in clayey materials (Kaabeche, 1996).

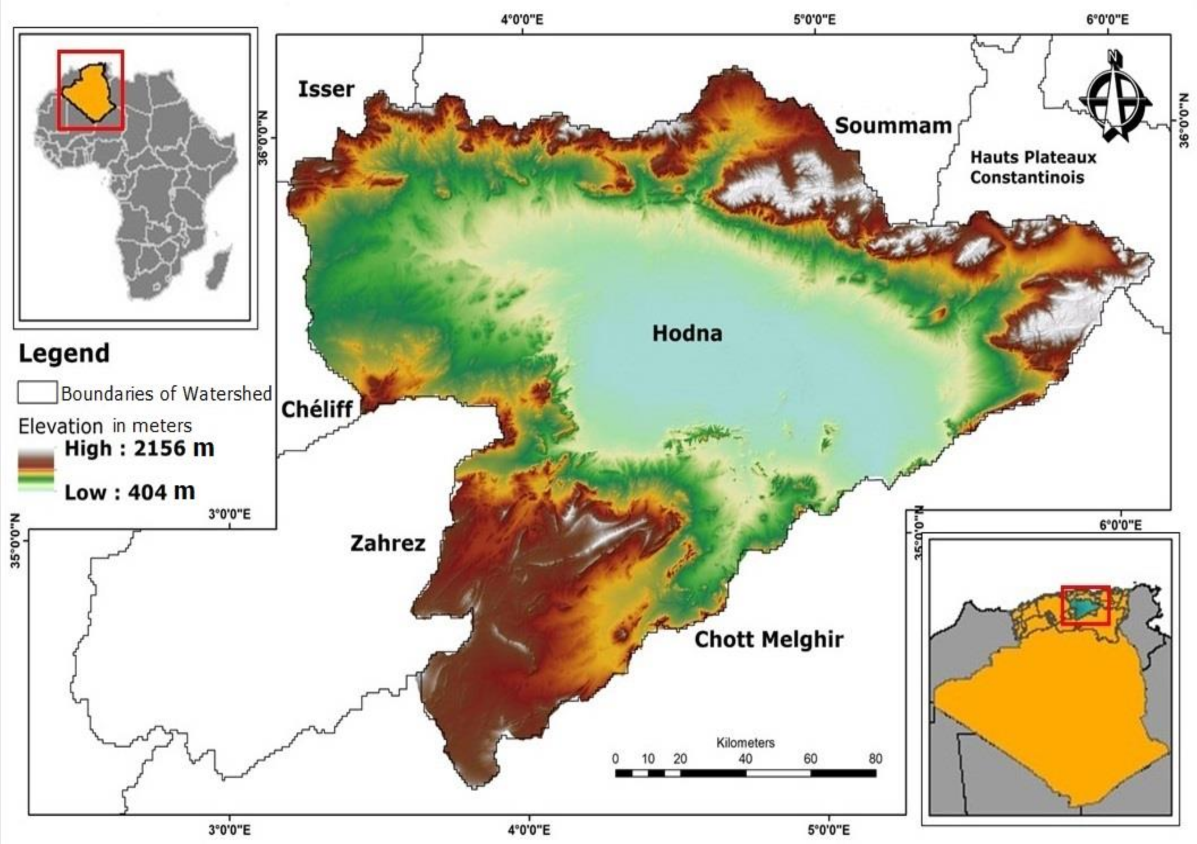

Figure 1: Representation of the Study Area

Materials and methods

Methods

The nature of the dependent and independent variables plays an initial guiding role in selecting a model. In the case of continuous dependent variables in nature, multiple linear regression can be used. When it is dichotomous in nature, as desertification phenomena defined by its presence or absence in a given terrain unit, discriminant analysis and logistic regression are suitable (Mathew et al., 2009). However logistic regression has been often used in various fields, it is preferable to discriminant analysis when the independent variables are categorical, continuous, or combined (Atkinson & Massari, 1998).

The logistic regression model is the most frequently applied model to depict the relationship between an outcome dependant or response variable and a set of independent predictive or explanatory variables (Smith & Mckenna, 2013). It is robust when the data are auto-correlated, which is the case for the Geographic Information System (GIS) raster coverages (Mathew et al., 2009). In a practical sense, unlike discriminant analysis logistic regression does not rely on strictly meeting the assumptions of multivariate normality and equal variance-covariance matrices across groups, which are often not met in many situations but logistic regression is much more robust when it happens, making its application appropriate in many situations and it has simple statistical tests, similar to approaches to incorporating metric and nonmetric variables and nonlinear effects, and a broad range of diagnostics (Joseph F. Hair et al., 2009). It does not only provide an assessment of how relevant a predictor is, but also its direction of association positive or negative. Based on these advantages, in our study of desertification susceptibility, it has been decided to use logistic regression where the dependent variable is dichotomous.

Logistic regression is a mathematical modelling approach that is based on the logistic function ρ , which is defined as:

$$\rho = \frac{1}{1+e^{-z}} \quad (1)$$

where ρ is the odds of the event occurrence that varies from 0 to 1, and z is the linear logistic model, that varies from −∞ to +∞, and can be defined as:

$$z = \alpha + \sum \beta_i X_i \quad (2)$$

Where:

α : is the constant,

β i: is the corresponding coefficient, and

X i: is the independent variable

Hence, z is an indicator that combines the independent variables. By substituting Equation (2) in (1), we get:

$$\rho = \frac{1}{1 + e^{-\alpha + \sum \beta_i X_i}}$$

using the data of the independent variables we estimate the unknown parameters of α and β_i, seeking the best fit by applying the maximum likelihood method. The observed data have a value of 0 or 1, meaning the occurrence or not of the hazard (Mathew et al., 2009).

Desertification factors (independent variables)

Desertification indicators highlight the processes of desertification to its endpoint of irreversibly barren soils. The most effective ones, nonetheless, are those which indicate the probable risk of desertification while there is still time and scope for remedial measures (Ferrara et al., 2020), in the light of that and based on key factors often used or referred to in the literature(Abahussain et al., 2002; D'Odorico et al., 2013; De Pina Tavares et al., 2015; Djeddaoui et al., 2017; Ferrara et al., 2020; Hadeel et al., 2010; Kairis et al., 2014; Kosmas et al., 2003, 2006; Mirzabaev et al., 2019; Rubio & Bochet, 1998) thirteen factors that seems suitable were selected for our watershed and divided into four categories as follow: Geomorphological, environmental, soil and socioeconomic factors and implemented as a resampled rasters using "R" (R Core Team, 2016) so they all get similar pixel size and same extent to avoid errors applying the logistic model that allows the use of binary and scalar values for the independent variables that are not continuous that is why we should encode binary values of 1 to relevant classes and 0 to remaining classes for each categorical variable (Dai & Lee, 2002). In our study all our factors are continuous except for the slope aspect raster which has a categorical form.

Geomorphological factors

Desertification and geomorphological processes are interwoven, involving several morphodynamic factors altering landforms such as soil erosion and serve as indicators of land degradation and hence play a significant role in desertification monitoring (Bakhit & Ibrahim, 1982), in Algeria erosion is a permanent calamity, the enormity of its direct and indirect consequences are difficult to translate into figures but easy to estimate (Benabbas, 2006). It represents a serious risk because of its permanent action over a long period and in large areas (Grecu, 2016). In an attempt to assess desertification, we identified six geomorphological predictive factors that play a major role in the desertification process used in previous studies (Basso et al., 2010; Djeddaoui et al., 2017; Ferrara et al., 2020; Kosmas et al., 2003; Wang et al., 2008).

Slope aspect is an important trigger for land degradation processes. It affects the microclimate by influencing the angle and the duration at which the soil is exposed to the sun leading to higher temperatures and increased evapotranspiration. South, West and Southwest-facing slopes receive more sunlight resulting in a drier soil prone to erosion and incapable of supporting vegetation. Reduced vegitative cover combined with the slope gradient gravitationall pull effect further exacerbates erosion stripping away rich topsoil accelerating desertification (Kosmas et al., 2003). A value of 1 was assigned for the target classes and a value of 0 for the rest of the aspect classes.

Slope gradient is one of the most critical factors recognized as affecting land degradation and desertification risk by exacerbating soil erosion (Kairis et al., 2014), which has a severe impact on soil and environmental quality (Lal, 2001). Steeper slopes are subject to an accelrated soil erosion and hydrological pattern alteration causing rapid runoff influencing the inflitration rates and the transport of sediments along with a reduced plant cover contributes to the desertification process.

Elevation is a significant factor with a direct impact on climatic conditions, mainly due to the changing patterns of precipitation and temperatures at different elevation gradients (Tai et al., 2020). The climatic variations induced by the elevation affects soil moisture and vegetative patterns combined with the slope aspect and gradient along with the soil composition may lead to resilient or vulnerable areas to desertification. In our study we used the "SRTM Plus version 03 "of 1 arc-second (30 m) digital elevation model (DEM) from the Shuttle Radar Topography Mission (Farr et al., 2007).

Topographic Position Index (TPI) is an important terrain attribute that reflects the erosion vulnerability, particularly in areas prone to tillage erosion (Wehrhan & Sommer, 2021). It influences plants distribution affecting moisture levels and environmental stressors exposition like wind and water erosion, TPI also shapes the livestock grazing distribution (Gersie et al., 2019). Additionally, TPI may be significant to the ecological traits of an area and its hydrology, mesoclimate or microclimate, wind exposure or cool air drainage at several scales (Weiss, 2001). TPI is the difference between the elevation at the center point (Z_C) and the average elevation (Z_A) across a defined radius (R) and calculated using the following equation (De Reu et al., 2013):

$$TPI = Z_C - Z_A$$

In order to compute the TPI in our case we used the ArcGIS (Esri, 2019) Geoprocessing tool called "Topography Tools" and applied a radius of (100 pixels) which we found to be more suitable for our watershed.

In the presence of streams and channels and their erodible effects, Drainage density is an important factor in the erosion processes (Akgün & Türk, 2011), quantifying the number of streams within a defined area unit (km²) it serves as an indication of erosion potential (Grecu, 2018) which contributes to desertification. High drainage density accelerates topsoil removal during rain events reducing soil productivity and limiting water infiltration exacerbating soil degradation and desertification. It is commonly used to assess both erosion and desertification. The drainage network was derived from a (30 m) resolution DEM and the drainage density was computed using a grid of rectangular polygon of (10x10 Km²) as a spatial extent within ArcMap (Esri, 2019).

Water Erosion is the predominant form of soil degradation, it occurs on all continents and under all climatic conditions. it manifests in two forms: the loss of topsoil through surface wash and terrain deformation. In areas with low structural stability run-off water may quickly incise gullies, washing away substantial soils. this process have several consequences for fertile topsoil reducing the productive potential of the soil (Oldeman, 1991) that leads to desertification.

In our study, we adopted the Revised Universal Soil Loss Equation (RUSLE) (Wischmeier & Smith, 1978) a well-known and universally accepted and implemented empirical soil erosion estimation model based on five factors (Ghosal & Das Bhattacharya, 2020) integrated with GIS to identify areas highly affected by water erosion using the following equation:

$$A = R \times K \times LS \times C \times P$$

Where:

A: computed spatial average soil loss per unit of area, expressed in ton per hectare per year ($t.ha^{-1}$ /yr).

R: the erosivity factor is defined as the product of kinetic energy and the maximum 30-minute intensity and displays the effect of raindrop impact and also shows the amount and rate of runoff associated with precipitation events (Wischmeier & Smith, 1978).

Given by the following equation developed by (Wischmeier & Smith, 1978) and modified by (Arnoldus, 1980):

$$\boldsymbol{R} = \sum_{i}^{12} 1.735 \times 10(1.5 \times log_{10}\left(\frac{\rho_i^2}{\rho}\right) - 0.08188)$$

where ***R*** is the rainfall erosivity factor ($MJ \cdot mm{\cdot}ha^{-1}{\cdot}h^{-1}{\cdot}y^{-1}$), ρ_i is the monthly rainfall (mm), and ρ is the annual rainfall (mm).

Rainfall monthly data was obtained from global land precipitation data of the Climate Research Unit by the University of East Anglia (CRU) version 4 (Harris et al., 2020) as a NetCDF file and using ArcGIS to extract the corresponding bands of the twelve months of 2018 and then use cell statistics to calculate the annual rainfall and converting the raster to points to be interpolated using the Kriging method to get our (30 m) resolution raster map for ***R*** factor.

K: is soil erodibility factor it is the rate of soil loss per rainfall erosion index unit ($t \cdot ha \cdot h{\cdot}ha^{-1}{\cdot}MJ^{-1}{\cdot}mm^{-1}$) and accounts for the effects of soil qualities on soil loss during storm events. It is connected to the combined effect of rainfall, runoff, and infiltration (K.G. Renard et al., 1997) and to calculate the soil erodibility factor we used (J.R. Williams, 1995) formula:

$$\boldsymbol{K} = F_{csand} \times F_{cl-si} \times F_{orgc} \times F_{hisand}$$

$$\boldsymbol{F_{csand}} = (0.2 + 0.3 \times \exp\left[-0.256 \times m_s \times \left(1 - \frac{m_{silt}}{100}\right)\right])$$

$$\boldsymbol{F_{cl-si}} = (\frac{m_{silt}}{m_c + m_{silt}})^{0.3}$$

$$\boldsymbol{F_{orgc}} = (1 - \frac{0.25 \times orgc}{orgc + \exp\,[3.72 - 2.95 \times orgc]})$$

$$\boldsymbol{F_{hisand}} = (1 - \frac{0.7 \times (1 - \frac{m_s}{100})}{\left(1 - \frac{m_s}{100}\right) + \exp\,[-5.51 + 22.9 \times (1 - \frac{m_s}{100})})$$

Where: ***Fcsand*** is a factor that confers low soil erodibility factors for soils high on coarse sand and high values for soils with small amount of sand, ***F(cl-si)*** is a factor that confers low soil erodibility factors for soils high on clay and silt proportions, ***Forgc*** is a factor that decreases soil erodibility for soils high on organic carbon content, ***Fhisand*** is a factor that decreases soil erodibility for soils with very high sand contents, ***msilt*** is the percentage of silt content (0.002–0.05- mm diameter particles), ***mc*** is the percentage of clay content (<0.002-mm diameter particles), ***ms*** is the percentage of sand content (>0.05- mm diameter particles)

Using a digital soil map of the world vector data of the FAO (Food and Agriculture organisation of the United Nations) from the FAO soil portal as an ESRI shapefile which also contains the data that concerns many properties of soil such as gain size (silt, clay and sand) and organic matter content, once the soil properties derived and the ***K*** factor is calculated we use it as a field value to convert the soil map of our watershed from polygon to raster to obtain soil erodibility raster map.

LS is the topographic factor slope length and steepness which interpret the effect of topography on erosion in RUSLE. We can also say that it determines the influence of landforms on soil erosion (Grecu et al., 2017), it is a combination of slope length factor (L) defined as the horizontal distance from the source of overland flow to the point where depositions begin or runoff becomes concentrated in channels and slope gradient factor (S) which reflects the influence of slope gradient on erosion (K.G. Renard et al., 1997).

The equation proposed by (Ian D. Moore & Gordon J. Burch, 1986) was adopted to calculate LS Factor:

$$LS = [Flow\ Accumulation \times \frac{cell\ size}{22.13}]^{0.4} \times [\frac{\sin Slope}{0.0896}]^{1.3}$$

Where: Flow accumulation indicates the accumulated upslope contributing area for a given cell computed along with slope steepness using DEM in ArcGIS, cell size is the size of the grid cell, in our case (30 m) and sin slope is the slope degree values in trigonometric function sin.

C: cover management factor most often used to compare the relative influence of management schemes on conservation plans, it reflects the impact of cropping and management practices on erosion rates (Renard et al., 1997). Ranging from a value of 0 indicating full soil coverage to a value of 1 indicating no soil coverage (Wischmeier & Smith, 1978), The factor C has been calculated using the NDVI (Normalized Difference Vegetation Index) derived from 30-meter resolution Landsat 8 OLI/TIRS Collection 2 Level-2 data during the 2018 growing season, and applying the formula used by Vatandaşlar & Yavuz (2017) on a semi-arid watershed as follows:

$$\boldsymbol{C} = 0.431 - 0.805 \times NDVI$$

P: conservation practices factor is the soil-loss ratio with a specific support practice to the corresponding soil loss with upslope and downslope plowing. practices that primarily affect erosion by altering the surface runoff parameters which reduces soil loss and consequently corrects the Soil loss estimation (K.G. Renard et al., 1997). Mostly applied for agricultural areas or artificial pastures and ranging between 0 and 1 and, where 0 refers to the highest effectiveness of the conservation practices implemented and 1 refers to the absence of support practices or measures.

In our study in the absence of conservated practices outside the agricultural lands which are poorly managed, we derived the ***P*** factor using the method proposed by Wischmeier & Smith (1978) that suggests assigning a certain ***P*** value according to slope percentage and land use cover type as follows:

Table 1: *P* values (Wischmeier & Smith, 1978)

Land use type	**Slope (%)**	***P* factor**
Agriculture	0-5	0.1
	5-10	0.12
	10-12	0.14
	20-30	0.19
	30-50	0.25
	>50	0.33
Other	All	1
Land use type	Slope (%)	***P*** factor

And for the land use map we used the ESA WorldCover, a global land cover product at 10 m resolution for 2020 based on the Sentinel-1 and 2 data with an overall accuracy of 73.6± 0.2 providing 11 classes and is defined using the Land Cover Classification System (LCCS) by the United Nations (UN) Food and Agriculture Organization (FAO) (Zanaga et al., 2021).

Wind Erosion is the second most significant type of soil degradation, it is an intricate geomorphological phenomenon omnipresent in arid and semi-arid regions where the vegetation is sparse and soil is often loose and dry making it a detrimental process as it leads to the loss of rich topsoil and also alters soil structure shaping dunes and blowouts that accelerates desertification.

In our study we implemented the Index of Land Susceptibility to Wind Erosion (ILSWE) adopted by (Borrelli et al., 2015, 2016) that relies on the combination of the following key factors: surface protection is minimal to non-existent, soil surface vulnerability and strong winds as a condition for wind erosion occurrence (Borrelli et al., 2015) and the equation is given as follows:

$$\boldsymbol{ILSWE} = CE \times EF \times SC \times VC \times SR$$

Where:

CE: is climatic erosivity factor, a measure of the climatic susceptibility to generate conditions conducive to wind erosion (Skidmore, 1986), calculated by the equation proposed by (Chepil et al., 1962):

$$\boldsymbol{CE} = \frac{386 \times u^3}{\boldsymbol{PE}^2}$$

with $\boldsymbol{u}$ as the mean wind speed (m/s) obtained from the "Global Wind Atlas 3.0" owned and operated by the Technical University of Denmark (DTU) and ***PE*** is the Thornthwaite potential evaporation index calculated as follows:

$$\boldsymbol{PE} = 3.16 \times \sum (\frac{P_i}{T_{i+22}})^{10/9}$$

where $\boldsymbol{P_i}$ is the monthly mean precipitation (mm); $\boldsymbol{T_i}$ is the monthly mean temperature (C°) derived from high-resolution grids of monthly climatic observations CRU-TS 4.03 dataset (Harris et al., 2014) statistically downscaled with WorldClim 2.1 (Fick & Hijmans, 2017).

EF: is the wind-erodible fraction of the soil that interprets the soil's capacity to withstand wind forces, it expresses the relationship between soil loss by wind and the characteristics of the soil surface (Fryrear et al., 1994).

We applied the equation based on the soil's texture and chemical proprieties proposed by (Fryrear et al., 1994) as follows:

$$\boldsymbol{EF} = \frac{29.09 + 0.31 \times \boldsymbol{SA} + 0.17 \times \boldsymbol{SI} + 0.33 \times \frac{\boldsymbol{SA}}{\boldsymbol{CL}} + 2.59 \times \boldsymbol{OM} - 0.95 \times \boldsymbol{CaCO_3}}{100}$$

where ***SA*** is the sand content, ***SI*** is the silt content, ***CL*** is the clay content, OM is the organic matter content and $\boldsymbol{CaCO_3}$ is the calcium carbonate content within the verified lower and upper threshold values specified by (Fryrear et al., 1994). We used data of topsoil in the digital soil map of the world vector data of the FAO to extract the soil proprieties.

SC: Soil crust is a relatively thin, consolidated layer at the soil surface, it is more compact and mechanically stable compared to the soil underneath (Zobeck, 1991), it is usually less vulnerable to abrasion by blowing soil and erodes at a slower pace than the soil beneath it (Fryrear et al., 2000). Playing a major role in conserving soils, it has been utilized to estimate the impact of soil crust on the wind erosion susceptibility of soils (Borrelli et al., 2014). We calculate it based on (Fryrear et al., 1998) equation:

$$\boldsymbol{SC} = \frac{1}{1 + 0.0066 \times (\boldsymbol{CL})^2 + 0.21 \times \boldsymbol{OM}^2}$$

where ***CL*** is the clay content and ***OM*** is the organic matter, and we used data of topsoil in the digital soil map of the world vector data of the FAO to extract these soil properties.

VC: Vegetation cover factor, for assessing wind erosion vegetation parameters such as height and foliage cover (leaf area) are essential (Wischmeier & Smith, 1978). The existence of a vegetated cover increases the turbulence close to the surface and therefore dissipates the wind's kinetic energy resulting in a decrease of the near-surface wind velocity (Shao, 2008) and subsequently a reduction in wind erosion, and to describe the vegetation cover we used the Leaf Area Index (LAI), an established index that is largely employed for modelling soil erosion by water (Shao Y; Leslie, 1997), we employed the "Biophysical Processor" developed for the SNAP toolbox to compute several biophysical variables to derive the (LAI) using Sentinel-2 level-2A product, Bottom Of Atmosphere (BOA) reflectance images (10 meters) resolution from September 2018.

SR: Surface Roughness factor, is important for the wind erosion assessment as it affects wind dynamics by enhancing frictional effects, which diminish wind energy near-surface (Wever, 2012), and therefore dissipating wind erosivity.

Applying the equation proposed by (Evans, 1972) using the raster calculator:

$$\boldsymbol{SR} = (FS_{mean} - FS_{min})/(FS_{max} - FS_{min})$$

Where FS_{mean}, FS_{min} and FS_{max} are mean, minimum and maximum focal statistic layers prepared using the DEM with the focal statistics tool from the neighborhood toolbox in spatial analyst tools within ArcMap, that calculates for each input cell location a statistic of the values within a specified neighborhood around it which in our case was 100 meters.

Environmental factors

Environmental factors play a key role in the desertification process as they can facilitate the assessment and monitoring of desertification at regional and local scales, by providing synthesized information on the state and trends of environmental processes that lead to desertification (Kosmas et al., 2003), in our study two factors have been retained as environmental predictive parameters of desertification: the NDVI and Evapotranspiration.

NDVI (Normalized Difference Vegetation Index) a simple numerical indicator that can be used by remote sensing measurements and one of the most extensively applied vegetation indices for its sensitivity to the presence, density, and condition of vegetation, it has been employed as an indicator of desertification in the literature (Ghebrezgabher et al., 2019; Lamchin et al., 2016; Lamqadem et al., 2018; Salih et al., 2021). Vegetation cover is a pivotal element in the desertification dynamics as it enhances soil stability and improves inflitration maintaining moisture levels and fertility mitigating arid conditions and land degradation susceptibility. We used the atmospherically corrected surface reflectance image Landsat 8 OLI/TIRS Collection 2 level-2 acquired on August 2018 to extract the NDVI of our watershed.

Evapotranspiration is the simultaneous loss of water from plants and soil surfaces to the atmosphere as a process. It consists of two distinct processes involved : transpiration and evaporation. Transpiration is water loss from the plants and evaporation is water loss directly from the soil surface or from evaporating surfaces other than plants (Novák, 2011). In our study we used the potential evapotranspiration, it provides a practical approach to evaluate the drought severity in some geographical regions, especially where water is the limiting factor affecting plants and soil productivity (Croitoru et al., 2013; Kosmas et al., 2003), increasing potential evapotranspiration led by any minor variation in meteorological factors induced by climate change increase dry conditions which may exacerbates desertification (Shan et al., 2016).

To derive the mean annual potential evapotranspiration map for our study we used the Potential ET (PET) layer provided in the year-end gap-filled 8-day composite dataset MOD16A2GF version 6.1 produced at 500 m pixel resolution and a scale factor of 0.1 which is the improved MOD16 (Running et al., 2021), extracted the corresponding layers of 2018 using the AppEEARS software (AppEEARS Team, 2022) and then used ArcGIS to calculate, extract and resample the layer to 30m resolution for the Hodna Watershed keeping in mind that raster resampling may not improve accuracy and is used just for the spatial alignment to help prevent issues such artifacts by standardizing the proprities of the rasters.

Soil Factors

Soil is a living medium resulting from the physical and chemical weathering of the parent rock under the influence of climatic and biological agents. It is an essential component that performs several ecological functions in ecosystems crucial for bioactivity. Today, soil degradation, including desertification, results from a reduction in the soil's ability to support these vital functions. This phenomenon is caused by various factors, including erosion, salinization, elemental imbalances, acidification, and depletion of soil organic matter (Lal, 2012; Allam et al., 2021). Soil texture, structure, organic matter content, mineralogy, water retention capacity, stone content, parent material, slope angle, aspect, climate, and rate of soil formation are parameters that influence the impact of soil degradation on desertification (Lahlaoui et al., 2017 ; Zouidi et al., 2019). Soil depth, in particular, remains a critical indicator of the current state and potential risk of desertification (Kosmas et al., 2003).

In our study we selected two predictors as soil factor influencing the desertfication process, the soil salinization considered to be one of the most relevant indicators to characterize desertification (Kibblewhite et al., 2007) with the NDSI (Normalized Difference Salinity Index) and the LST (Land Surface Temperature) which is a crucial parameter for earth surface as it is sensitive to vegetation and soil moisture, therefore it can be used to detect desertification (Javed Mallick & Bharath, 2008).

NDSI (Normalized Difference Salinity Index) is a numerical indicator used in remote sensing to quantify the soil salinization. An important manifestation of land degradation (Yu et al., 2022), a mechanism in arid and semi-arid climatic zones refering to the accumulation of water soluble salts (NaCl) in topsoil to a level that leads to the decline of agricultural production and ecosystem productivity (D'Odorico et al., 2013). We apply the formula proposed by (Khan et al., 2001) to calculate NDSI as follow using Landsat 8 OLI/TIRS Collection 2 level-2 acquired on August 2018 bands:

$$NDSI = \frac{(Red - NIR)}{(Red + NIR)}$$

Where Red and Near Infrared (NIR) are the Bands 4 and 5 respectively of the Landsat 8 OLI/TIRS bands.

LST (Land Surface Temperature) is the radiative skin temperature of the land obtained from solar radiation, it is a measurement of thermal radiation emitted from the land surface when incoming solar energy interacts with and heat up the ground or the canopy surface in vegetated zones (Khan et al., 2021).

LST is a decisive factor in the physical processes of surface energy and water balance it is widely used in numerous fields including evapotranspiration, climate change, hydrological cycle and vegetation monitoring (Li et al., 2013) that is why it gets a fundamental importance in the study of desertification, in our case we derived the LST from the Landsat 8 OLI/TIRS Collection 2 level-2 acquired on August 2018 using the following equation (Avdan & Jovanovska, 2016):

$$T_s = \frac{BT}{\{1 + [(\lambda BT/\rho)\ln \varepsilon_\lambda]\}}$$

Where:

T_s is the LST in Celsius, *BT* is at-sensor brightness temperature (C°) given as follow:

$$BT = \frac{K_2}{\ln[(K_1/L\lambda) + 1]} - 273.15$$

With K_1 and K_2 as the band-specific thermal conversion constants from the metadata file and Lλ is the top of atmospheric (TOA) spectral radiance given as follow:

$$L\lambda = M_L * Q_{cal} + A_L - O_i$$

Where M_L represents the band-specific multiplicative rescaling factor (0.0003342), Q_{cal} is the Band 10 image, A_L is the band-specific additive rescaling factor (0.10000), and O_i is the correction for Band 10 (0.29)

λ is the wavelength of emitted radiance for Landsat 8 band 10 which is equal to 10.8

ε_λ is the land surface emissivity calculated with the equation used by (Sobrino et al., 2004) as follow:

$$\varepsilon_\lambda = 0.004 * P_v + 0.986$$

Where P_v is the vegetation proportion obtained according to (Carlson & Ripley, 1997):

$$P_v = \left[\frac{NDVI - NDVI_{min}}{NDVI_{max} - NDVI_{min}}\right]^2$$

And ρ is the velocity of light $\boldsymbol{c}$ (2.998×10^8 m/s) divided by the Boltzmann constant (1.38×10^{-23} J/K) $\boldsymbol{\sigma}$ multiplied by the Plank's constant $\boldsymbol{h}$ (6.626×10^{-34} J s)

$$\rho = h \times \frac{c}{\sigma}$$

Socio-economic Factors

According to (Geist & Lambin, 2004) the climatic conditions operating simultaneously or synergistically with socioeconomic driving factors is the most widespread mode of causation of desertification and its underlying dynamics, the contribution of the socioeconomic aspect was dominant and accounted for a larger portion of the overall effect with the human activities and livestock as robust drivers of desertification (Feng et al., 2015).

In the light of that we choose to implement in our study the human influence index map to describe human activities using a methodology outlined by (Sanderson et al., 2002) and the livestock map of our area of interest extracted from the Gridded Livestock of the World (GLW 3) (Gilbert et al., 2018) that can be used later for the assessment.

Human Influence Index Map (HII) is the combined influence of several factors yielded via an overlay of continuous raster data layers that represent the various factors presumed to exert an impact on ecosystems and its values range from 0 no human influence to 64 with maximum human influence (Table 2).

In the case of our region of interest, we excluded coastlines and navigable rivers as such elements do not exist. For the Land cover, we used ESA WorldCover (Zanaga et al., 2021) and that same layer was used to extract urban polygons while for the Rail and Major roads, we used the global roads open access data set version 1 (CIESIN, 2013) and the night-time stable lights

values was derived using NASA's Black Marble night-time lights product suite (Román et al., 2018) which provides estimates of daily night-time lights (NTL) and other intrinsic surface optical properties.

Table 2: Implemented factors and their respective scores

Influence of Population density/Km²	**Score of influence**	**Influence of Railroads**	**Score of influence**
0 - 0.5	0	Within 2 km of railroads	8
0.6 - 1.5	1	Beyond 2 km of railroads	0
1.6 - 2.5	2	Influence Score of Major Roads	/
2.6 - 3.5	3	Within 2 km of roads	8
3.6 - 4.5	4	Within 2 to 15 km of major roads	4
4.6 - 5.5	5	Beyond 15 km of major roads	0
5.6 - 6.5	6	**Influence of Night-time Stable Lights Values**	**Score of influence**
6.6 - 7.5	7	0	0
7.6 - 8.5	8	1-38	3
8.6 - 9.5	9	39 - 88	6
> 9.5	10	>=89	10
Land Cover Categories	**Score of influence**	**Urban Polygons**	**Score of influence**
Urban areas	10	Inside urban polygons	10
Irrigated agriculture	8	Outside urban polygons	0
Rain-fed agriculture	3	**Influence of Coastlines**	**Does not apply for our study area**
Other cover types including forests	0	**Influence of Navigable Rivers**	**Does not apply for our study area**

In the case of our region of interest, we excluded coastlines and navigable rivers as such elements do not exist. For the Land cover, we used ESA WorldCover (Zanaga et al., 2021) and that same layer was used to extract urban polygons while for the Rail and Major roads, we used the global roads open access data set version 1 (CIESIN, 2013) and the night-time stable lights values was derived using NASA's Black Marble night-time lights product suite (Román et al., 2018) which provides estimates of daily night-time lights (NTL) and other intrinsic surface optical properties.

Livestock is one of the most significant socioeconomic factors as the effect of overgrazing is devastating the plants and the soil, it reduces the canopy cover, damages topsoil structure and compacts the soil due to trampling which leads to soil crusting that in turn reduces soil infiltration and increase soil erosion vulnerability (Yong-Zhong et al., 2005; Merdas et al., 2021). We use the Gridded Livestock of the World (GLW 3) database (Gilbert et al., 2018) reflecting the most recent subnational livestock distribution statistics for 2010. Cattle, buffaloes, horses, sheep, goats, chickens, and ducks are all represented as global population densities in each land pixel at a spatial resolution of 0.083333 decimal degrees, derived in a single raster layer for our study area. To ensure consistency with other rasters, we resampled the GLW data to meet a 30m resolution. a necessary resampling for spatial alignment that may lead to a loss of information. Regarding temporal resolution, although the GLW data refers to 2010 and other parameters cover slightly different time frames (2018), we suggest that this small difference is acceptable but does imply certain limitations.

The dependent variable

In order to evaluate the logistic model using a dependent variable and due to the lack of updated cartographic data and maps of desertification sensitivity we decided to use the NDVI anomalies as NDVI effectiveness on monitoring land cover changes has been proven (Sternberg et al., 2011). Negative changes that occur suggest drought, land degradation and desertification conditions because the degradation of the vegetative cover represents an important factor that numerous researchers include in their definition of desertification. As the cover density decreases, the risks of wind and water erosion, the adverse effect of excessive solar radiation on bare soils and surface reflectivity are increased dramatically, which contributes significantly to the desertification processes(Glantz & Orlovsky, 1983).

Forum geografic. Studii și cercetări de geografie și protecția mediului
Volume **XXIII**, Issue **1** (**June 2024**), pp. **16-43**; DOI: **10.5775/fg.2024.1.3629**

For the NDVI anomalies, we used the terra moderate resolution imaging spectroradiometer (MODIS) vegetation Indices (MD13Q1) Version 6.1 with 250 m spatial resolution (Didan, 2021). We took the NDVI of 2018 and compared it to the average NDVI decade from 2008-2017 using raster calculator we applied a scaling factor 0.0001 and used the following formula:

$$NDVI_{Anomaly\ 2018} = NDVI_{2018} - NDVI_{avg(2008-2017)}$$

As for the training datasets, it is recommended to use the best sampling method which is equal proportions of 1 for the presence or 0 for the absence of phenomena in the entire study area (Ayalew & Yamagishi, 2005) for the same pixel values of the independent variables, for our study, we distributed randomly 1800 points using stratified random sampling, 900 points where the NDVI anomalies were positive or hadn't undergone any changes as a sign of no desertification, and another 900 points where the NDVI anomalies were negative as a sign of desertification to be merged as a binary dichotomous data in a single raster layer with each pixel assigned 1 for desertification and 0 for non-desertification and that's what the logistic regression model requires to generate a susceptibility map, subdivided as 66% and 33% training dataset for the regression analysis and validation dataset for the accuracy assessment respectively.

Logistic regression model implementation

Once the dataset containing the independent variables and the dependent variable was generated for the same area which is the Hodna watershed the logistic regression analysis was carried out using "R" (R Core Team, 2016), "Rstudio"(RStudio Team, 2015), "Raster Package" (Hijmans & Etten, 2012), "Rgeos Package"(Bivand & Rundel, 2021),"ROCR Package"(Sing et al., 2015) and "Rgdal Package"(Bivand & Keitt, 2017).

Upon using the "gml" function the regression coefficients were obtained (Table 3) we then used an accuracy assessment for the overall predicted accuracy and used the pR2 function for the goodness of fit test with McFadden's, Cox & Snell's and Nagelkerke's pseudo-R^2 as an outcome. For the multicollinearity diagnosis we used the function "ols_vif_tol" to derive Tolerance "TOL" and the Variance Inflation Factor "VIF" an important index widely used for that matter(O'Brien, 2007) and for the correlation between the dependent and independent variables we rely on the ROC curve as a quantitative measure for the model's accuracy.

Results and discussion

Overall statistics

The table below shows the main outputs from the logistic regression and the calculated Odds Ratio, the independent variables "Predictor" used in the model, the regression coefficients "Estimate", the "Standard Error "of the regression coefficients, the test statistic of significance "Z value" and the p-value "Pr(>|z|)".

Table 3: Estimated coefficients of the logistic model

Variables	Estimate	Standard Error	Z value	Pr(>|z|)	Odds Ratio
Intercept	2.666e+01	4.747e+00	5.617	1.95e-08	3.57e+11
Aspect	7.610e-04	8.970e-04	0.848	0.039625	1.00e+00
Drainage Density	-1.143e+00	3.158e-01	-3.621	0.000294	3.19e-01
Elevation	-4.284e-03	5.378e-04	-7.966	1.64e-15	9.96e-01
Evapotranspiration	2.538e-05	1.518e-04	0.167	0.687155	1.00e+00
HII	3.526e-02	1.591e-02	2.217	0.026624	1.04e+00
Livestock	9.653e-05	5.689e-05	1.697	0.089725	1.00e+00
LST	3.188e-01	6.388e-02	4.991	6.02e-07	1.27e+00
NDSI	5.346e+02	3.561e+00	1.501	0.013336	2.10e+02
NDVI	5.217e+02	3.558e+00	1.466	0.014262	1.84e+02
Slope	1.553e-02	3.102e-02	0.501	0.616693	1.02e+00
TPI	2.442e-02	2.085e-02	1.171	0.241473	1.02e+00
Water Erosion	-2.091e-04	2.051e-04	-1.019	0.308100	1.00e+00
Wind Erosion	1.994e+00	1.118e+00	1.784	0.047404	7.34e+00

The coefficients are statistically significant and associated with a p-value <0.05 so our model suggests that most of the predictors do affect desertification susceptibility.

The predictors (Slope, TPI, Livestock, Evapotranspiration, Water and Wind erosion) have a p-value over the 0.05 threshold. As for the odds ratio we got predictors with an odds ratio equal to 1 which indicates a neutral association for the desertification susceptibility, these predictors are (Aspect, Elevation, Evapotranspiration, Footprints, Livestock, Slope, TPI and water erosion) and predictors that have an odds ratio less than 1 indicating a negative association with the desertification susceptibility which are the (Drainage density and the LST) and predictors greater than 1 indicating positive association with desertification susceptibility and these are (NDSI, NDVI and wind erosion). In addition, the accuracy assessment (Table 4) for the predicted validation dataset was calculated using "R" software with 0.74% for the presence of desertification and 0.66% for the absence of desertification with an overall accuracy of 0.70% which is acceptable.

Table 4: Accuracy assessment of the validation dataset

n=600	Predicted 0	Predicted 1
Actual 0	True Negative "199"	False Positive "101"
Actual 1	False Negative "77"	True Positive "223"
Accuracy	70%	

Table 5: Pseudo R² test of the logistic model

Pseudo R^2 Test	Value
McFadden R^2	0.165
Cox & Snell R^2	0.204
Nagelkerke R^2	0.272

For the goodness of fit we have calculated three Pseudo R^2 (Table 5) starting with McFadden R^2 with a value of 0.165 that does not fall far from the 0.2-0.4 range which after (Louviere et al., 2000) is representing a very good fit, the Cox & Snell R^2 and the Nagelkerke R^2 values are 0.204 and 0.207 respectively, all of these acceptable Pseudo R^2 values suggests that the predictor variables may be able to explain the response variable.

In terms of multicollinearity diagnosis we have calculated the Variance inflation factor (VIF) and the Tolerance (Table 6), the VIF ranges between 1.07 for the TPI to 2.52 for the Slope and the Tolerance ranges between 0.41 for the Elevation to 0.93 for the TPI, as a rule of thumb by (O'Brien, 2007) the multicollinearity is determined to be serious or excessive only if the VIF is greater than 4 or equivalent to a Tolerance level of 0.10 or 0.25 which is not the case here.

Table 6: Multicollinearity diagnosis index

Variables	Tolerance	VIF
Aspect	8.741975e-01	1.143906
Drainage Density	5.912450e-01	1.691346
Elevation	4.112777e-01	2.431447
Evapotranspiration	7.251566e-01	1.379012
HII	8.985054e-01	1.112959
Livestock	7.942807e-01	1.259001
LST	6.563278e-01	1.523629
NDSI	7.307631e-01	1.368432
NDVI	7.304922e-01	1.368939
Slope	3.969588e-01	2.519153
TPI	9.333138e-01	1.071451
Water Erosion	4.818443e-01	2.075359
Wind Erosion	4.390408e-01	2.277693

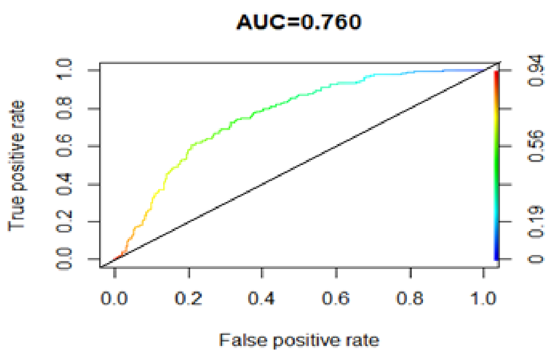

Figure 2: Receiver Operating Characteristic (ROC) curve

We also used the ROC curve graph, a useful technique used to visualize the model's performance (Fawcett, 2005) which is shown in the (Figure 2) and Area Under Curve (AUC) which measures the performance of the model across discrimination thresholds, the value of 0.760 is obtained for our study, while an AUC value of 1 is a sign of a perfect fit the 0.760 indicate an acceptable fit and implies a good correlation amongst the dependent and independent variables, as for the ROC graph we can notice that the proportion of correctly classified samples is greater than the proportion of incorrectly classified samples.

Predictive factors

Elevation induces a climatic effect on vegetation which is essentially caused by the changing patterns of precipitation and temperatures at different altitudes, at low elevations precipitation is scarce and temperatures are high which leads to high evapotranspiration and causes drought that limits the vegetation growth and at higher elevations precipitation increases, temperature drops, drought stress subsides and the vegetation growth accelerates (Tai et al., 2020) in our endoretic basin the higher elevations starting from "970" up to "2156" meters represented by the mountains of both the Atlas Tellian and Sahraoui with only 26% of the total area of the basin followed by an average elevation starting from "660" to "970" meters for 32% and ending at a vast depression, a flat area surrounding and including the Chott El Hodna for a 42% of the total area from "660" meters down to "404" meters with more than 23% under 520 meters (Figure 3A) which leads us to believe that at least 42% of the basin is subject to rainfall scarcity, high temperatures, drought and increased evapotranspiration thus the decline of the vegetative cover that leads to desertification.

Slope gradient substantially influences the amount of surface water runoff and soil sediment loss, when the slope angle exceeds a critical threshold, the rate of soil erosion increases which is the primary cause of land degradation and desertification (Kosmas et al., 1999). Our slope gradient map shows that most of the Hodna watershed has a slope angle not exceeding 8°degrees, with only higher slopes surpassing 15°degrees up to 68° degrees on the Tellian Atlas represented by the mountains of the Hodna est-ouest with the 1890 m of "Djebal Guetiane" decreasing down to 1000 m to the west and the Atlas Saharan in the south and southeast up to "1200" meters and around the region of Boussada at the piedmont of the mountains of Ouled Nail (Figure 3C).

Drainage density importance as an indicator lies in the measure of the network texture and reveals the balance between the erosive intensity of overland flow and surface soil resistance (DESERTLINKS, 2004), in our study area, the drainage density (Figure 3D) ranges from "0.11" km/km² to "3.1" km/km² which is considered poorly drained typical for an endorheic arid and semi-arid basin where the water drains to inland in the form of temporary lakes that evaporates leaving place to salt as it is the case for the "Chott El Hodna" at the center of our basin and a poorly drained soil is very vulnerable to salinization and desertification (Kosmas et al., 1999) but less susceptible to erosion processes.

Topographic Position Index (TPI) is the most important predictor after elevation as it affects the environmental characteristics (Weiss, 2001). In our basin it ranges from "-79.49" negative indicating valleys, upland drainages and lower slopes which based on (Weiss, 2001) might have a greater response to extreme weather events and up to "98.13" positive indicating high ridges and small hills with in between flat plains and open slopes ranging from "-2 to 6" and covers most of the area, the kind of landform with high sensitivity to grazing and human activities which have a major impact on land degradation and desertification (Figure 3E).

Slope Aspect, the Hodna watershed being an endorheic basin presents a varied topography with the Tellian Atlas to the north and northeast and the Saharan Atlas to the south, surrounding a flat area known as Hodna Chott. By observing the map (Figure 3F), it is noticeable that most areas in our basin face south, southeast, and southwest, indicating higher sun intensity. These areas experience greater stress in terms of moisture and biomass production, leading to desertification, as suggested by the slight violet hues.

Water erosion makes the soil vulnerable when the rate of soil loss is greater than the rate of the soil-forming process causing a progressive land degradation leading to a fragile ecosystem and subsequently to desertification (López-Bermúdez, 1990). The result of our RUSLE soil erosion map (Figure 5) of the Hodna watershed is consistent with the result of (Djoukbala et al., 2022) showing lowest soil loss rate by water is less than 50 $ton.ha^{-1}.yr^{-1}$ in most of the area, we can attribute that to the combination of low LS-factor (Figure 4B) as it gets as low as "3.18" areas with low values are predominantly flatter regions with minimal flow accumulation indicating reduced vulnerability to erosion and the low rainfall erosivity R-factor (Figure 4E) at the value of 116.7 $MJ\, mm\, ha^{-1}.h^{-1}.yr^{-1}$ mainly in the South-Est part of the basin. The highest soil loss rate by water exceeds "700 $ton.ha^{-1}.yr^{-1}$" concentrated in the high altitudes of the basin and correlated with high values of the LS-factor which reveals apparent patterns related to the hydrology and topography of the region, high values are observed along steep slopes and important drainage channels indicating areas with significant erosion potential, these regions align concentration of water flow and the steepness of the terrain as well as the R-factor. wetter regions with steep topography induce more surface runoff, transporting away the soil particles dislodged by the transfer of the kinetic energy of raindrops which is the primary physical agent of erosion (Verstraete & Schwartz, 1991).

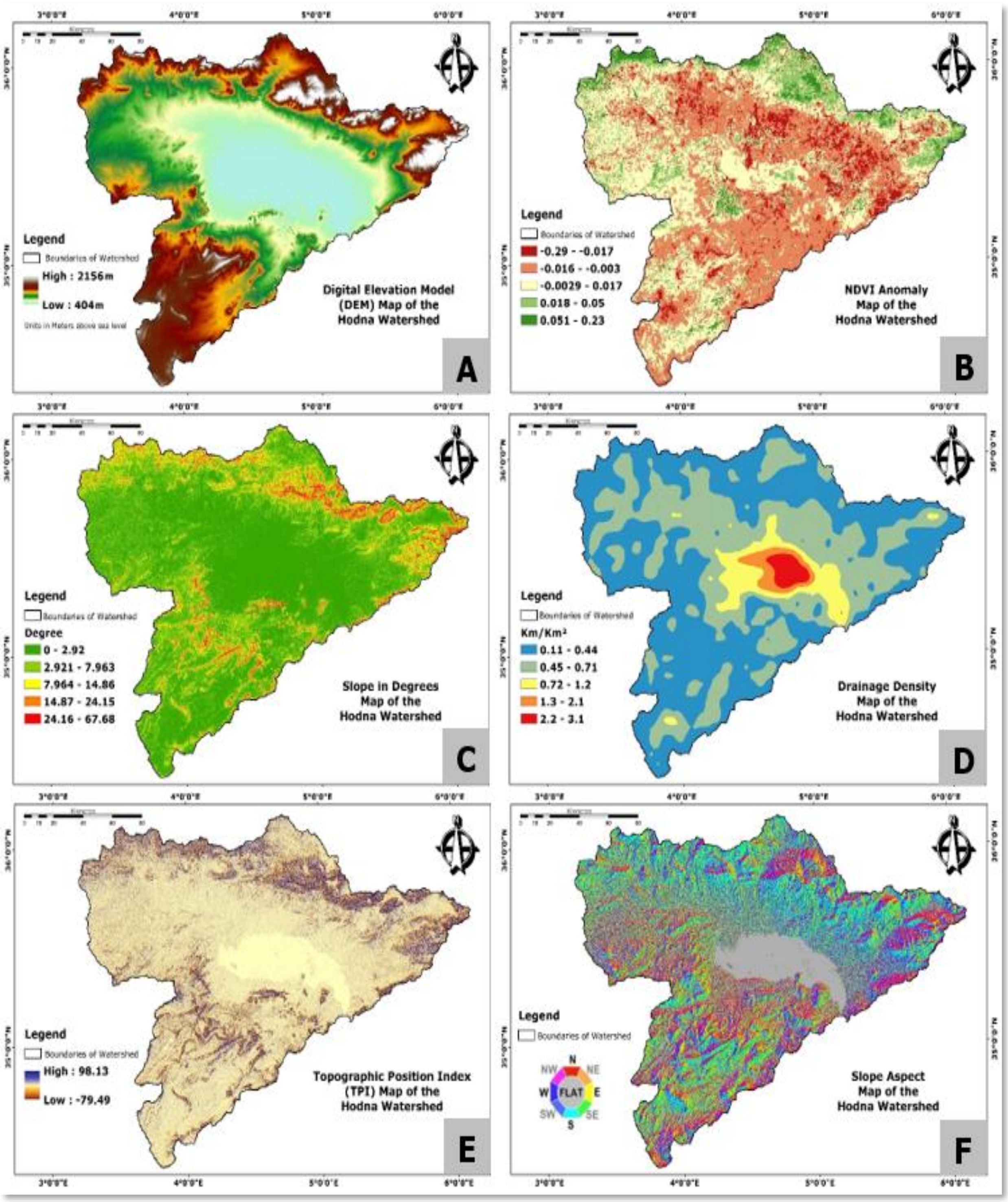

Figure 3: DEM (A), NDVI Anomaly (B), Slope (C), Drainage Density (D), TPI (E) and Aspect Maps of the Hodna Watershed

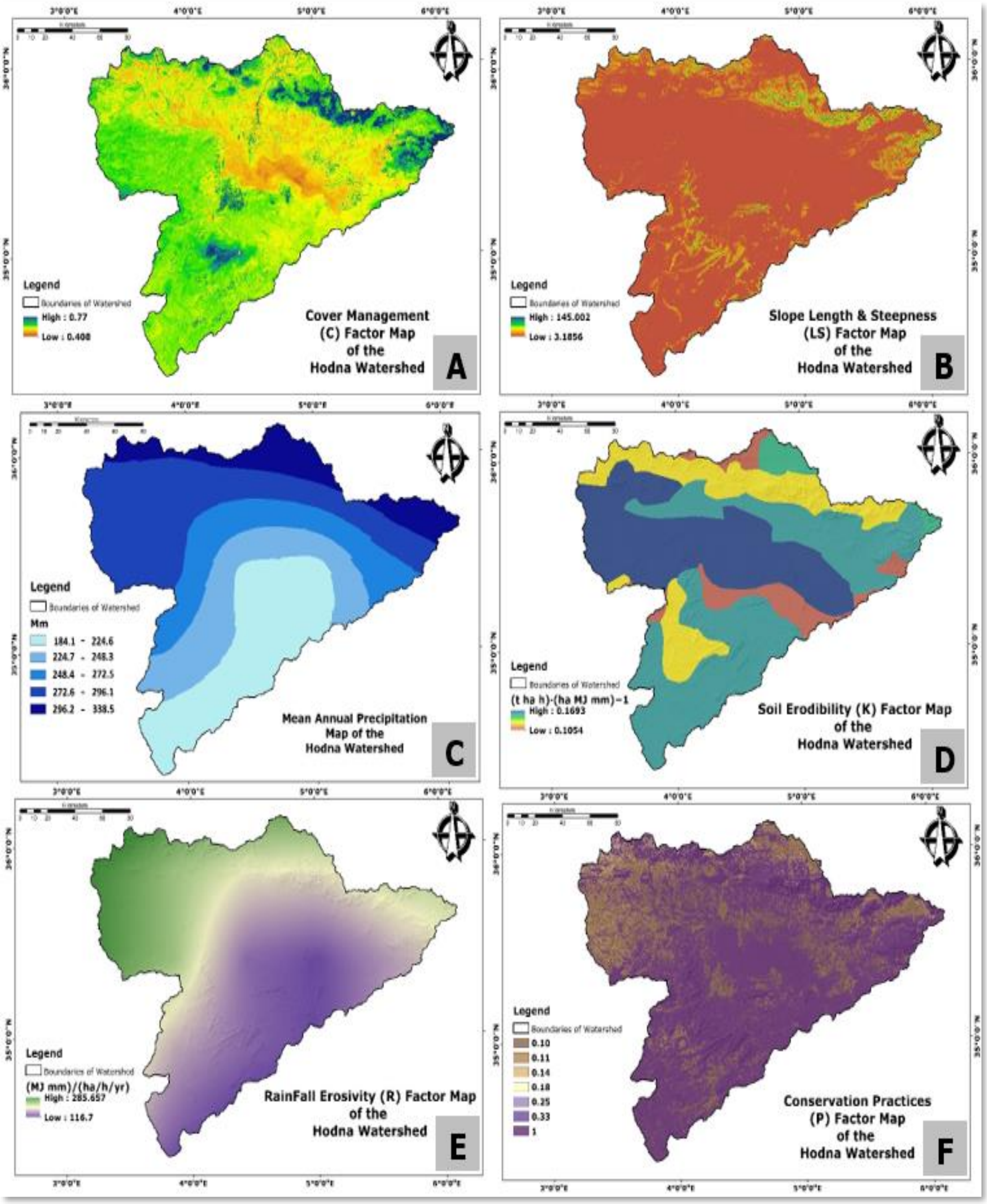

Figure 4: C Factor (A), LS Factor (B), Mean annual Precipitation (C), K Factor (D), R Factor (E) and P Factor (F) Maps of the Hodna Watershed

In addition to that, the soil erodibility K-factor (Figure 4D) standing for the erosion susceptibility and the rate of surface runoff which in our case ranges from 0.1054 to 0.1693 with values between 0.1054 and 1200 falling into the low category and depicted by the orange and yellow colors, values from 0.1200 to 0.1400 are classified as moderate while values ranging from 0.1401 to 0.1693 indicating higher susceptibility represented as a gradient of green and blue . most of our region of interest is falling within the moderate and high rates exacerbated by the low rates of P-factor (Figure 4F) conservation practices and the C-factor (Figure 4A) cover management.

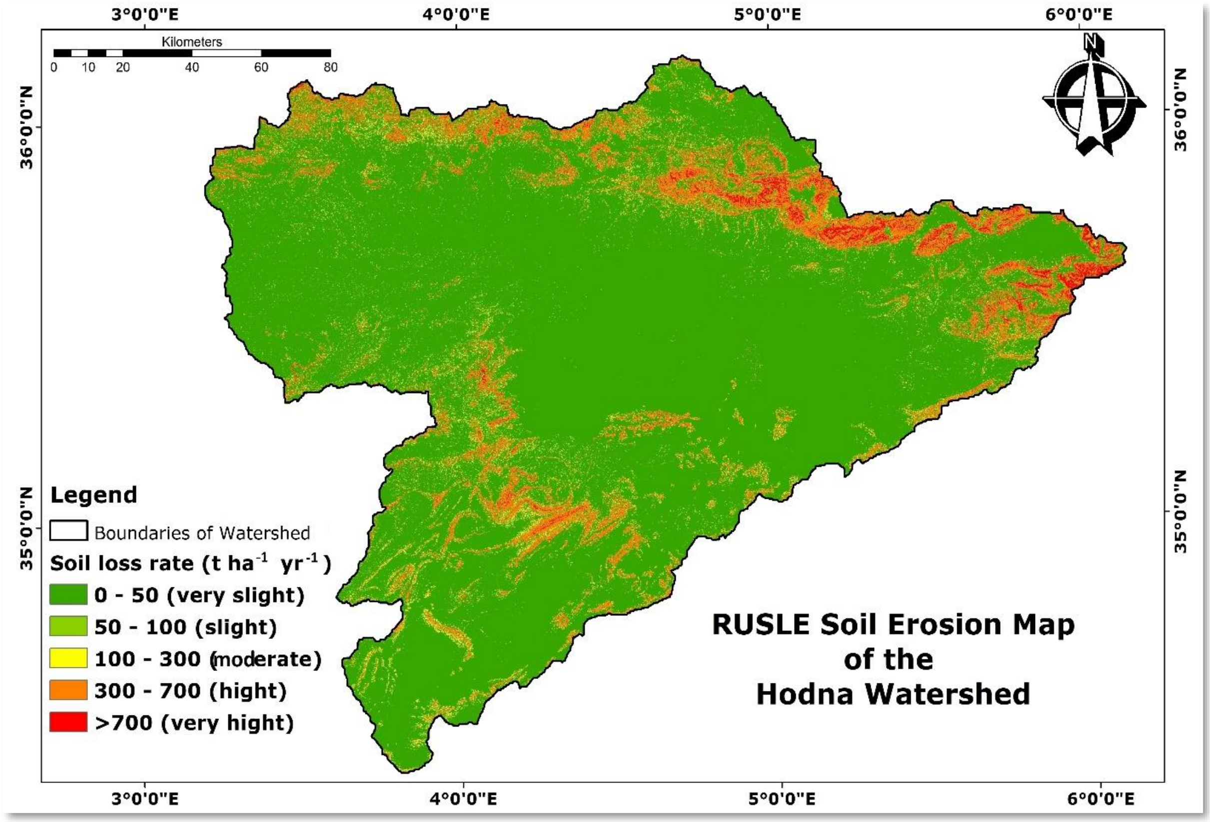

Figure 5: RUSLE Soil Erosion Map of the Hodna Watershed

Wind Erosion physically removes the fertile topsoil affecting land productivity with the soil erodibility known to be the primary cause for that phenomenon (Skidmore, 1994), in our study area the wind erosion susceptibility map (Figure 7) shows that 67% of the Hodna basin is undergoing a very slight susceptibility due to the low wind erodible fraction shown in the map (Figure 6C) where it has only high values West and North-West because of the prevailing winds in the Hodna basin is blowing in that same direction (Boureboune & Benazzouz, 2009) also the low climate erosivity factor (Figure 6A) being high only around Chott El Hodna at the center and from there extending to the south while the rest of the basin is mostly low highlighted with blue color to moderate green and then yellow approaching to the center towards the south. Only 2% of the total surface of the basin have a high susceptibility to wind erosion located in elevated areas where the wind erodible fraction is high and the wind velocity there is greater compared to near-surface one. Whereas 31% of the total area of the basin is having slight to moderate susceptibility to wind erosion mainly due to the fact that all the contributing factors in these areas implies more tendency towards more wind erosion susceptibility, that portion of the basin have a low soil crust CS factor (Figure 6E) making the soil less compact and mechanically instable and the fraction of vegetative cover FVC (Figure 6D) is negative which represents the two main protecting layers against wind erosion.

Surface ridges as shown by the surface roughness map (figure 6F) are not very present in our basin based on the nature of its relief where it is mostly flat except for the high-altitude areas of the basin extending from Est to West towards the Hodna mountains and South on the Atlas Saharan chain, flat surface ridges mean lesser effect on reducing wind energy and dissipating wind erosivity. The land use land cover map compared to the wind erosion susceptibility map shows that Built-up areas and grasslands are the most sensitive areas to wind erosion, the built-up areas due to the human activities and the grasslands are highly influenced by and vulnerable to wind erosion (Zou et al., 2021).

“NDVI” Normalized Difference Vegetation Index (Figure 8A) negative values represent water bodies while Rocks, sands and built-up concrete surfaces gets close to zero and positive values ranging from 0.1 to 0.5 represent sparse vegetation and forests are higher than 0.6 (Jones & Vaughan, 2010) for our area of interest the NDVI is ranging from -0.18 to 0.55 where more thant 85% of the basin have a very low vegetative cover or is a barren soil as it is the case at Chott El Hodna where we can find the lowest values as the NDVI highlights the amount and vigor of that vegetation. There’s no dense vegetation since the highest value is only 0.55 which represents croplands, shrubs,grasslands and a sparse cover of cedar trees at the eastmost of the basin around the region of Batna’s province up until the Maadid range north-east Msila’s province and around 35 hectares of Pine and Oak trees located south in Boussaada at the "mountain of Messaâd". A low vegetative cover makes our basin more vulnerable and susceptible to desertification and could be interpreted as a desertification's onset due to the crucial role that it plays such as reducing raindrop splash effect, improving topsoil organic matter,soil stability,water holding capacity, hydraulic conductivity and reducing surface runoff (Kosmas et al., 1999).

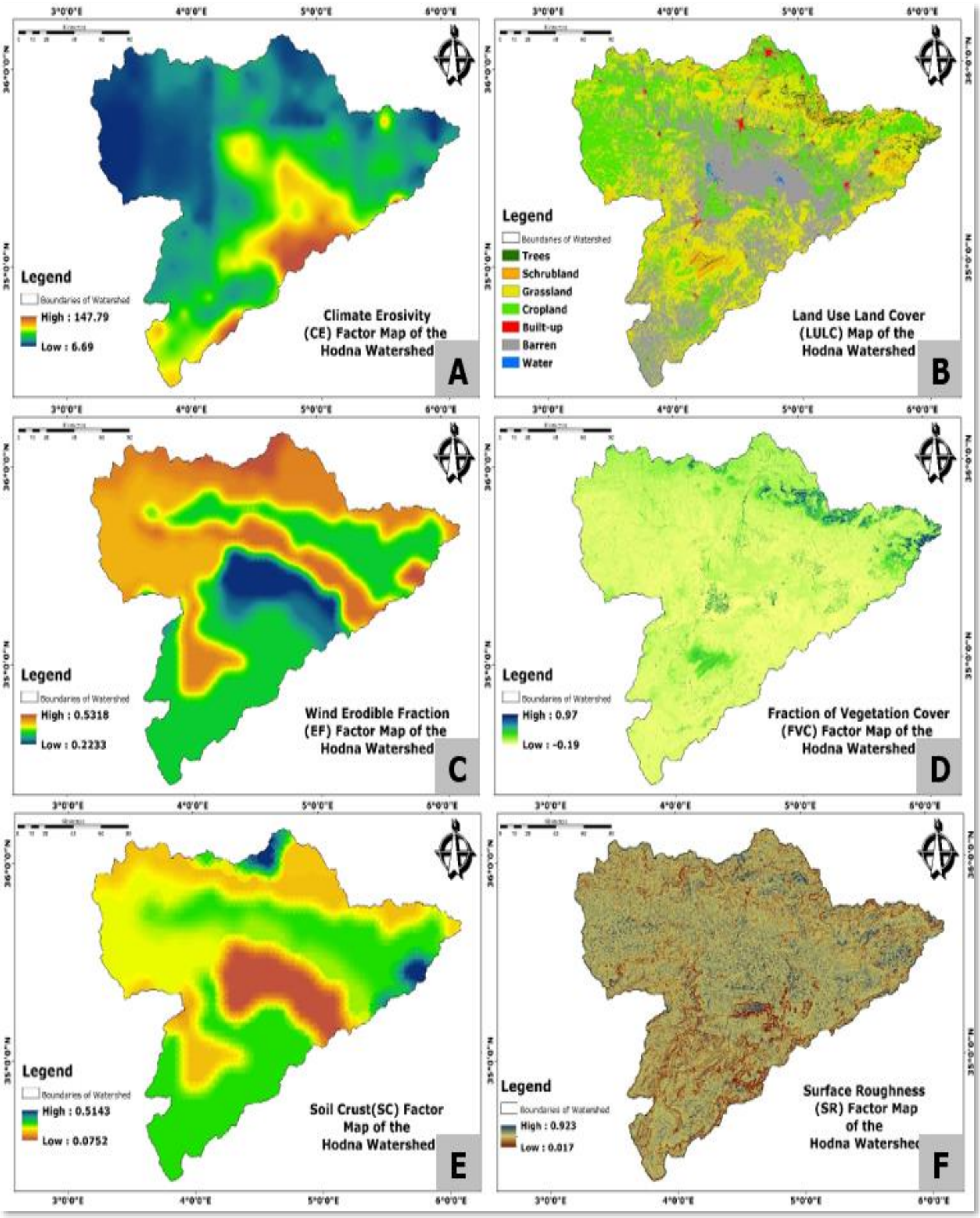

Figure 6: CE Factor (A), LULC (B), EF Factor (C), FVC Factor (D), SC Factor (E) and SR Factor (F) Maps of the Hodna Watershed

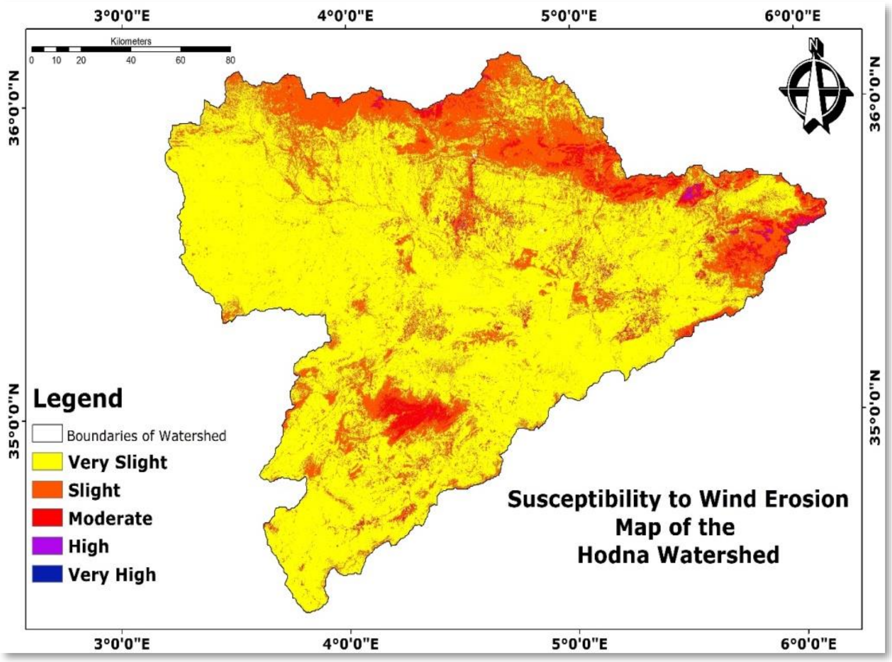

Figure 7: Susceptibility to Wind Erosion Map of the Hodna Watershed

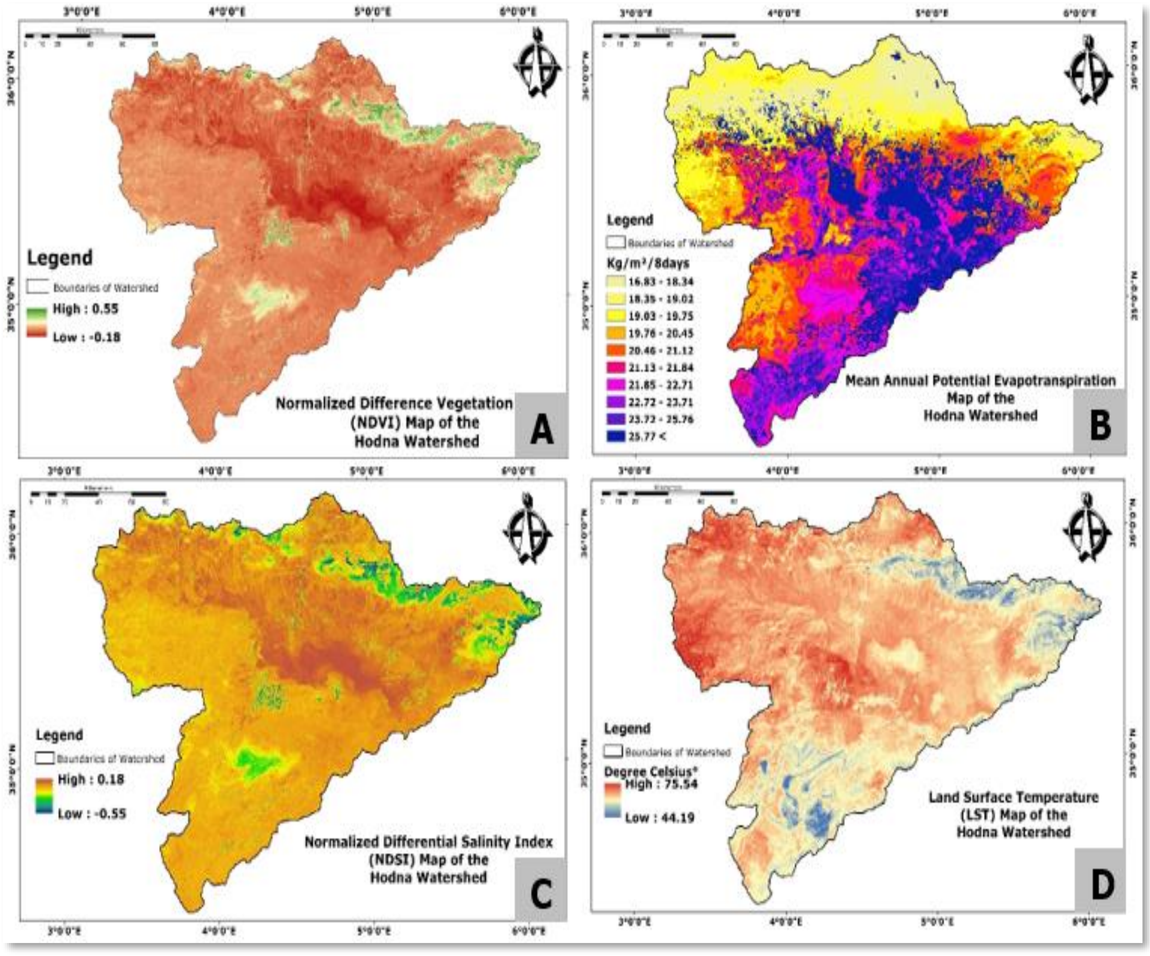

Figure 8: NDVI (A), Mean Annual Potential Evapotranspiration (B), NDSI (C) and LST (D) Maps of the Hodna Watershed

Forum geografic. Studii și cercetări de geografie și protecția mediului
Volume **XXIII**, Issue **1** (**June 2024**), pp. **16**-**43**; DOI: **10.5775/fg.2024.1.3629**

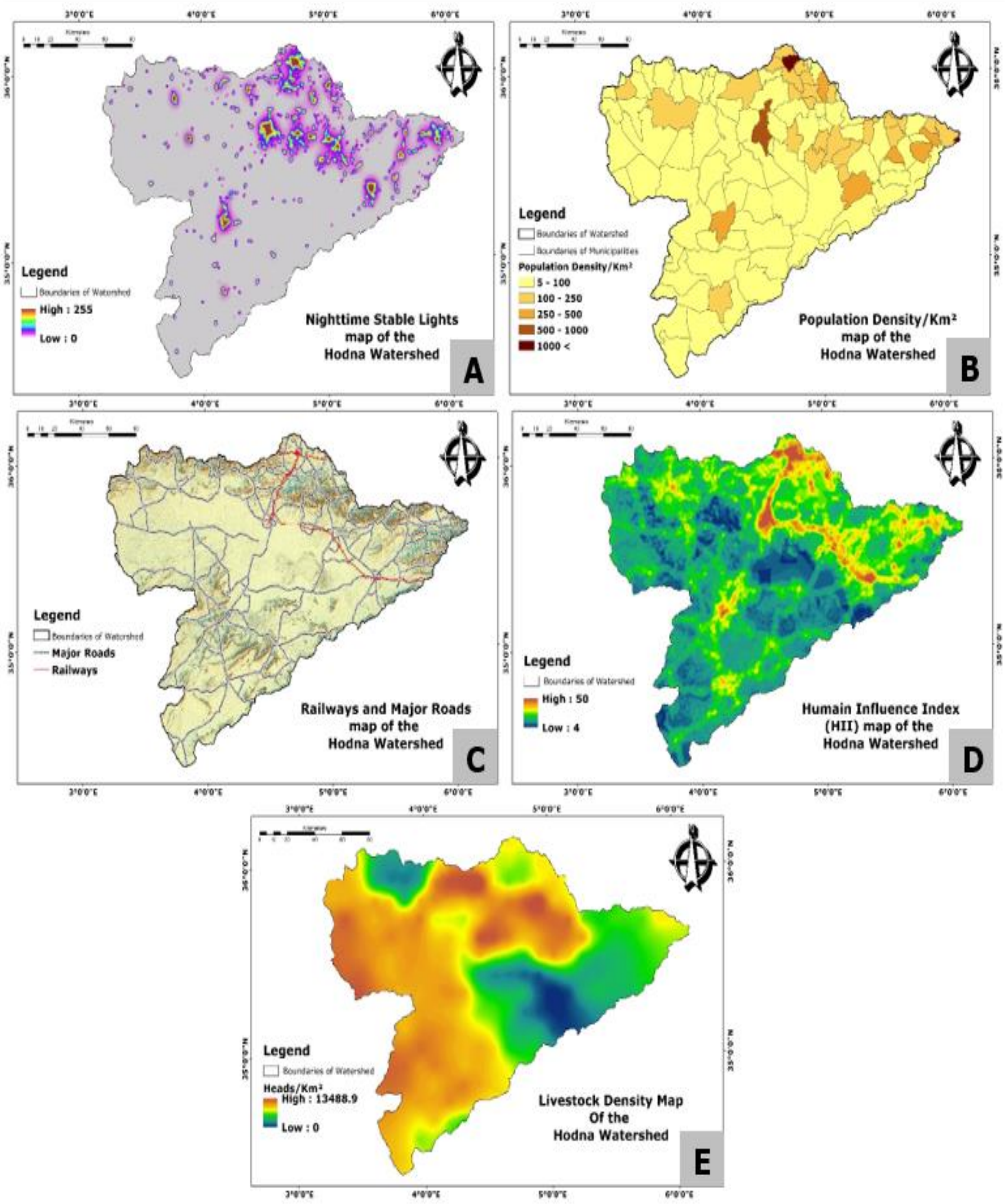

Figure 9: Nighttime Stable Lights (A), Population Density (B), Railways and Major Roads (C), Human Influence Index (D) and Livestock Density (E) Maps of the Hodna Watershed

Evapotranspiration (Figure 8B) is ranging from 16.83 Kg/m²/8days to more than 25.88 Kg/m²/8days where the lowest values are in the northmost part of our basin and the higher values are in the southmost and south-east part, in this case the lowest evapotranspiration losses does not occur in the drier south part where the average annual precipitation is under 250 $mm.yr^{-1}$, knowing that the climatic conditions affecting the evapotranspiration are: humidity, wind speed, air temperature and solar radiation (Allen et al., 1998) and with the highest levels of evapotranspiration occurring in the south of our basin this could be explained by the amount of solar radiation, where based on our slope aspect map the highest values are found in the center at the saline lake Chott El Hodna towards the southmost and south-east parts being prone to more solar radiation, in addition to that we can relate to the drainage density map where the areas with moderate to higher drainage density have higher values of evapotranspiration, a network of shallow wadis that are sensitive to climatic variations because shallow surface waters are more susceptible to climatic pattern changes (Musy, 2005).

"NDSI" Normalized Difference Salinity Index (Figure 8C) shows that our basin is highly affected by salinization except for the elevated areas with a dense vegetative cover and the agricultural lands, soil salinization is mainly a soil degradation process exacerbating desertification in plain areas and lowlands undergoing poor drainage conditions (Kairis et al., 2022) which is the case for our basin especially in Chott el Hodna, an endorheic salt lake fed by the wadis flowing from the Atlas Tellian North, wadis that frequently overflows and salinize the soil once evaporated due to rainfall irregularities.

LST Land Surface Temperature (Figure 8D) obtained from the Landsat 8 OLI/TIRS during the month of August 2018 where we assumed there will be higher temperatures to be recorded during the year, it is ranging from 44.19° up to 75.54° which is extremly high due to the low soil moisture and the excessive solar radiation characterising arid and semi-arid regions and highlighted by the slope aspect for our study area especially in the middle barren area of Chott El Hodna extending to the West with the lowest values only on elevated areas with North-facing slopes.

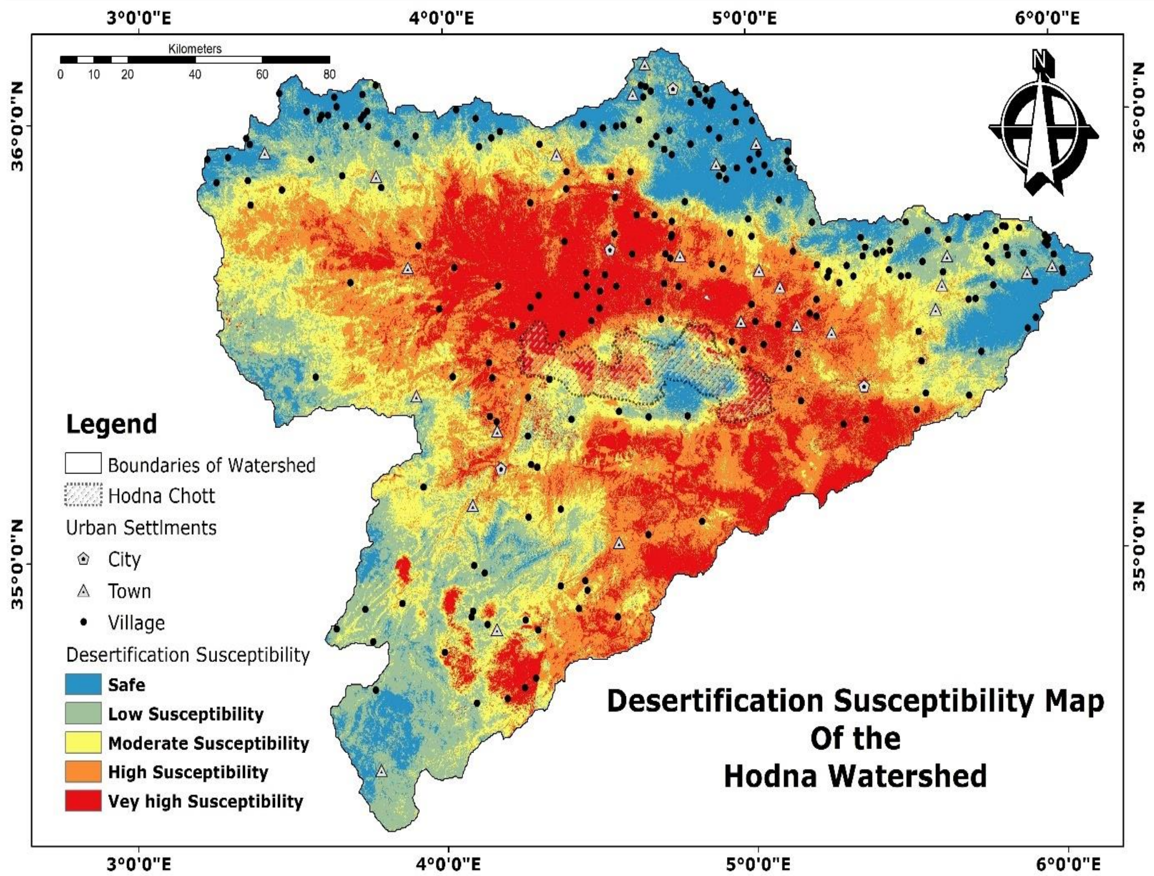

Figure 10: Desertification Susceptibility Map of the Hodna Watershed

In the southern part of the watershed, despite the presence of areas characterized by low Land Surface Temperature (LST) there is significant water vapor loss through evaporation emphasized by the high mean annual potential evapotranspiration (PET), such condition could be explained by the local topography and the vegetative cover which favors substantial moisture levels since the area is the forest of Djebel Messaad of aproximately 33500 Hectares with mainly Pine and Oak trees and a culminating mountain peak of Djebel Fernane at 1680 meters above sea level.

Human Influence Index Map HII (Figure 9D) scores range from a minimum of 4 indicating less human influence to a maximum of 50 reflecting a greater degree of influence with 43% of the total basin having a considerable index which represents mainly important urban settlements being the most densely populated municipalities (most of the municipalities of Bordj Bou Arreridj province North, Msila at the center with Ouled Derradj and Souamaa, Boussaada and Ain Melh South, Sidi Aissa and Chellalat El Adhaoura West and Barika,Taxlent, N'gaous, Merouana East a part from Batna's Province) having more than 100 habitants per Km², these urban settlements are also within 15 Km of major roads or less and 2Km from railroads and with sufficient night-time stable lights brightness to be detected by satellite.

Livestock (Figure 9E) is very high up to more than 10000 heads per square Kilometres in major part of our basin between the Atlas Tellian and the Atlas Saharan in the Algerien steppes known for being the typical place of livestock breeding and grazing with most of the national herd, on the North at the piedmont of the Atlas Tellian in Msila's province and its surrounding municipalities such as El Maadid and Hammam Edalaa and from there extending to the West and South of the Chott El Hodna expanding towards the Atlas Saharan.

Predicted susceptibility map of desertification

After several tests, the natural breaks classification method proved to be the most suitable for mapping desertification susceptibility, mainly because it is a form of variance-minimization classification where breaks are usually uneven, and features are divided in a way that classes boundaries are set depending on large changes occurring in the data values (Longley et al., 2007). Ranging from 0 to 1 the desertification susceptibility raster was divided into five classes (Safe, Low, Moderate, High and Very Hight) susceptibility as shown in (Figure 10) 13.2% of the total area designated to be safe, low and moderate susceptibility zones represent 20.3% and 21% respectively, high and very high susceptibility zones constitutes 25.4% and 20% respectively.

Discussions

Predictive Factors

Based on previous studies and literature we selected thirteen predictive factors presumably appropriate for predicting desertification, we obtained a raster map for the zones with a certain degree of susceptibility to desertification ranging from safe to very high sensitivity. The resulting map is acceptable as the predicting model went thru several statistical evaluations for both the quality of prediction and its stability, starting with the p-value seven out of thirteen of the predictors have a p-value < 0.05 therefore they are statistically significant and a remaining of six predictors with a p-value >0.05 bypassing the significance threshold doesn't necessarily imply that these are not good predictors it could be due to the fact that these predictors has been emphasized already in other parameters by the model to avoid double consequences or they have a little impact on the desertification. After that instead of interpreting the logistic model coefficients we've calculated the odds ratio as its interpretation is preferable it displays the constant effect of the predictive factors, based on the odds ratio estimated it was obvious that the NDSI, NDVI and Wind Erosion with odds ratio of 2.10e+002, 1.84e+02 and 7.34e+00 respectively plays a major role on the likelihood that desertification will occur but it is noteworthy that the values of the odds ratios for the NDSI and NDVI might be overestimated and that could be explained by the fact the training dataset used the NDVI anomalies which also uses the red and near-infrared bands as the NDVI and NDSI and to address this issue of that possible degree of multicollinearity or correlation we used the Tolerance and VIF indicators, with Tolerance above 0.04 and VIF below 2.5 meaning that multicollinearity is not a significant issue here and we recommend further investigations or alternatively taking in consideration if available the use of desertification dataset that is less correlated with the NDVI and NDSI than NDVI anomalies.

As for the multicollinearity diagnosis, the tolerance values are above 0.4 and VIF values are below 2.5 which is are acceptable thresholds meaning that multicollinearity is not an issue except for the Slope variable with a tolerance and VIF equals 0.3969 and 2.519 respectively which indicates that it might be correlated with other variables in the model, however there are some variables with tolerance values above the conventional threshold 0.4 but lower than 0.5 such as Elevation, Water and Wind erosion which might be moderately correlated with other variables in the model.

Slope aspect has positive coefficient estimate of 7.610e-04 and a p-value of 0.39625 suggesting that it is statistically significant but with an odds ratio of 1.00 implying negligible or no relevant changes occurring which could be translated to a weak association due to the fact that Aspect highlights the amount of solar radiation impacting vegetation growth and soil moisture therefore desertification likelihood, that influence of the Aspect could have been already mediated in LST or Evapotranspiration. The Slope aspect has a negative effect on the biomass as it represents the angle and the duration of the sun's rays impact on the soil's surface with higher evaporation and erosion rates, slower vegetation regrowth for the south, south-eastern and south-western facing aspects (Kosmas et al., 1999).

Slope gradient has a positive coefficient estimate of 0.01553 but a p-value 0.617 over the threshold suggesting that the variable is not statistically significant in the prediction of desertification and with an odds ratio of 1.02 there is almost no changes occurring, it could be explained by the fact that the major role of the slope in the erosion process could have been already emphasized by the other variables such as water erosion, in the other hand the main socio-economic factors occur in low slope areas as abrupt slopes limits anthropogenic access and activities and the fact that our basin is an endoreic flat depression with more than 85% of its area under 8° slope angle.

Elevation has a negative coefficient of -4.284e-03 indicating higher elevation areas are less susceptible to desertification, high altitudes tend to have cooler temperatures and more rainfall which is the case for our basin nevertheless the erosion processes shouldn't be neglected, with a statistical relevant p-value of 1.64e-15 and negligible occurrence with an odds ratio of 9.96e-01 that can be translated to a one-unit increase in elevation decreases the desertification probability by 0.4%, a weak relationship due to the fact that it could has been already emphasized in another variable such as TPI.

Topographic position Index TPI has a positive coefficient estimate 0.02442 meaning that higher TPI values are correlated with slightly high desertification probability, it should be oppositely correlated as areas with higher TPI are generally hilltops and ridges they have more tendency for water availability and soil moisture retention supporting the vegetative cover better than areas with lower TPI such as depressions with low water and moisture retention making them vulnerable to waterlogging and salinization increasing the desertification probability, in our case that correlation could be explained by the erosion processes. The p-value of 0.24 indicating a significant association but with an odds ratio of 1.02 implying insignificant changes occurring.

Drainage Density has a negative coefficient estimates -1.143e+00 and a p-value of 0.000294 suggesting that higher drainage density is associated with lower probability of desertification occurrence with an odds ratio of 0.319 meaning that an increase in drainage density is associated with a decrease in the desertification susceptibility. That limited influence and negative impact could be explained by the nature of that drainage network being in an endoreic basin in a semi-arid region with a non-permanent and irregular flow inducing a limited impact of surface runoff and therefore limiting the influence of the erosion on desertification, in some other regions the drainage density could have a positive relationship with desertification where the potential role of surface runoff and erosion could have a major impact on its occurrence.

The analysis suggests a weak association between water erosion and desertification, the water erosion coefficient -2.091e-04 is statistically insignificant, the p-value 0.30 and odds ratio 1.00 provides no evidence that links water erosion and desertification susceptibility. However, the lack of a connection does not diminish its potential role. the model might attemp to avoid multicollinearity with factors like wind erosion, evapotranspiration, elevation, aspect and slope by omitting that variable's influence. The intercation between these variables might negate the real impact of water erosion, to improve future studies it is important to choose carefully the variables to prevent redundancy so that each variable adds up unique information to the model. Wind Erosion has a positive coefficient estimate of 1.994e+00 meaning a one unit increase in wind erosion increases the desertification susceptibility by 1.994 units, but based on the p-value that is equal 0.074 falling slightly above the conventional significance level of 0.05 which does not necessarily imply weak or insignificant association and may still indicate a meaningful association as statistical significance does not always reflect practical or substantive relevance and the odds ratio of 7.43e+00 with positive coefficient and the odds ratio suggests a positive relationship between wind erosion and desertification probability.

NDVI has a positive coefficient estimate 5.217e+02, a statistically significant p-value 0.014 and odds ratio 1.82e+02 implying that an increase in NDVI is associated with an increase in the log odds of desertification susceptibility. However, It is known that vegetative cover decreases with soil degradation leading to desetification therefore NDVI should theoretically be inversely correlated with the desertification susceptibility, a probable explanation could be the NDVI Anomalies used due to the lack of data as a dependent variable along with the NDVI acting as a confounding variables leading to biased estimates that distorts or confuses the relationship reflecting the positive correlation and the limitations of that alternative.

Evapotranspiration coefficient estimate is 2.538e-05 very close to zero with an odds ratio of 1.00 and p-value of 0.68 suggesting that this variable is not statistically significant, the PET raster has undergone a resampling process to align with the 30m resolution of the other layers to facilitate consistent spatial analysis it does not improve its accuracy and we aknowledge this limitation which could be one of the reasons that this variable is not statistically relevant. it could also be that this is not a good predictor or that its effect has already been mediated by another variable such as LST.

NDSI coefficient estimate is 5.346e+02 implying an increase in NDSI is associated with an increase in desertification susceptibility with an odds ratio equal to 2.10e+02 and a statistically significant p-value of 0.013.

LST coefficient estimate is 3.188e-01 indicating that the cooler the area is the less susceptible to desertification but with a slight effect as the coefficient is close to zero with statistical evidence of the association having p-value equal 6.02e-07 and odds ratio equal 1.27 meaning that for a one unit increase in the LST the odds of the outcome increase by a factor of 1.27.

Human Influence Index coefficient estimate is very small in the order of 3.526e-02 indicating a slight correlation with the desertification susceptibility and a p-value equal to 0.02 implying statistical significance however the odds ratio of the order of 1.04 indicating no relevant changes occurring, a possible explanation for that is that developed areas with high human activities could exacerbate the desertification susceptibility but it also could mitigate its effect if the adequate preventing actions and resources are implemented, however it is a complex relationship and a possible alteration of the variable contribution to the model cannot be neglected since the variable uses the land use land cover layer same as the wind erosion.

Livestock coefficient estimate is very close to zero 9.653e-05, for a one unit increase in livestock the changes occurring are negligible even though the p-value of 0.08 and odds ratio of 1.00 indicate no significant correlation with the desertification susceptibility, several reasons could explain that, it is possible that the livestock didn't capture well the grazing intensity which is in a direct relation to desertification or simply because it have been mediated by other variables such as drainage density, elevation or the human influence index as these are closely related to food and water availability. However its important to mention the limitations of the spatial resolution for that variable as the resampling process could induce inaccuracies or loss of details, similarly the discrepancy of the temporal resolution might affect the results and interpretations.

Desertification susceptibility Map

To conduct a qualitative and quantitative assessment of our desertification susceptibility map, we compared our probabilistic results with those from other studies on desertification sensitivity in the same region. Although their methods and factors differ from ours, we used the study by Boudjemline & Semar (2018) and Alliouche & Kouba (2023) applying the MEDALUS model (Kosmas & Ferrara, 1999), and Benslimane et al. (2009) using MODIS for Algeria, which includes our area of interest. We began with a visual analysis for qualitative comparison due to the lack of spatial data in these studies. Overall, our map aligns with their findings in the northern Tellian Atlas, particularly from the northeast to the northwest, including the Guetiane and Boutaleb mountains, the Mansoura mountain north of Hammam Dalaa province, up to the Dirah mountain north of Sidi Aissa province. To the east, it includes the Refaa mountain, and to the south, the Messaad and Fernane mountains, which form the northern part of the Saharan Atlas. These areas exhibit sensitivity levels ranging from safe to low, influenced by their topography, as the terrain plays a major role in precipitation, temperature, and wind patterns on the windward and leeward sides of the mountains, thereby affecting vegetation.

Regions at the piedmont of the mountains such as Sidi Aissa and Hammam Dalaa north, N'gaous and Sefiane East and Ain El Melh south have a moderate sensitivity to desertification followed by the regions that are flat extending towards the depression of "Chott El Hodna" having a high sensitivity to desertification such as M'sila, Magra, Barika, BenSrour, Boussada, Ain El Hadjel and the south of Ain El Melh.

For the quantitative analysis, we will use the study by Boudjemline & Semar (2018), as it focuses on the same region of interest ensuring an accurate and meaningful comparison. The study used factors similar to our model and classified desertification sensitivity into four categories: absent, low, moderate, and high. In contrast, our study classified desertification sensitivity into five categories. For the purpose of this comparison, we will assume that the 'high' and 'very high' categories on our map correspond to the 'high' category in their results. It turns out that the percentage of areas classified as safe is 13.2%, which is lower than the value mentioned in the previous study, 20.28%. Additionally, the percentage of high sensitivity on our map is 20.3%, which is higher than the value indicated in the other study, 10.48%.

The proportion of the land that have a moderate sensitivity is 21% while the value reported by the previous study is 50% and the proportion of the high and very high sensitivity is 25.4% and 20% making together a 45.4% which is greater than the high sensitivity value reported by (Boudjemline & Semar, 2018) of 17.42%, these noticeable differences could be explained by the fact that this study used a different amount of variables nevertheless there could be another explanation, we can observe by comparing the values of the different classes that the absence and moderate classes of the sensitivity in the first study when compared with the safe and moderate classes of our study has decreased while the low, high and very high classes sensitivity proportions of our study have increased, it could be explained by the fact that the timespan between the two studies was enough so that an exacerbation of desertification sensitivity in the Hodna watershed happened due to the climate change, precipitation scarcity and the anthropic pressure expansion. (Boudjemline & Semar, 2018) results used the precipitation data from 2014, the population density data of 2008, Landsat TM satellite image of 2009 and the map of the bioclimatic floors by FAO in (1972) while all the data we used are from 2018 and above.

Conclusions

The desertification susceptibility map of the Hodna watershed shows that most of it is prone to desertification hazards and land degradation as more than 40% of its area is subject to high and very high susceptibility while only 13.2% is considered to be safe and moderate to low susceptibility represents 20.3% and 21% respectively.

Furthermore, factors such as wind erosion, NDVI and NDSI which are more closely related to vegetation, land cover, and climate, also correspond to geomorphological, environmental, and soil factors are the most influential variables for our study area, while the least influential are the socio-economic factors. In addition, the reliableness of our model was validated by the area under the ROC curve showing good accuracy with 0.760 referring to a predictive accuracy of 76% also passing the uncertainty tests confirming the validity of the prediction, proving that the logistic regression is a practical tool in assessing the presence or absence of desertification. In our work, we simply identified the areas sensitive to desertification with an original contribution including variables that weren't adopted in previous studies for that region as wind and water erosion in detail not just as soil erosion and using NDVI anomalies to compensate for the lack of desertification data, providing an updated map of areas susceptible to desertification in an important watershed in Algeria for a better decision making process, however we recommend using numerical analysis of the contribution of each variable for a more precise selection as there are variables that we were certain of their contribution but in the study, they were non-significant, especially for the socio-economic factors which highlight the necessity of finding other ways to grasp their effect for a better hazard assessment.

Funding

This research received no external funding.

Author contribution

Conceptualization, T.K.; methodology, T.K., M.C. and M.Y.; formal analysis, C.B., F.G and M.C; investigation, T.K. and M.Y; writing—original draft preparation, T.K.; writing—review and editing, C.B. and F.G and M.C.

All authors have read and agreed to the published version of the manuscript." Authorship must be limited to those who have contributed substantially to the work.

Conflicts of interest

The authors declare no conflict of interest.

References

Abahussain, A. A., Abdu, A. S., Al-Zubari, W. K., El-Deen, N. A., & Abdul-Raheem, M. (2002). Desertification in the Arab Region: analysis of current status and trends. *Journal of Arid Environments*, *51*(4), 521–545. https://doi.org/10.1006/jare.2002.0975

Akgün, A., & Türk, N. (2011). Mapping erosion susceptibility by a multivariate statistical method: A case study from the Ayvalik region, NW Turkey. *Computers and Geosciences*, *37*(9), 1515–1524. https://doi.org/10.1016/j.cageo.2010.09.006

Albalawi, E. K., & Kumar, L. (2013). Using remote sensing technology to detect, model and map desertification: A review. *Journal of Food, Agriculture & Environment*, *11*(2), 791–797.

Allen, R. G., Pereira, L. S., Raes, D., & Smith, M. (1998). *Crop evapotranspiration - Guidelines for computing crop water requirements*. FAO - Food and Agriculture Organization of the United Nations. https://www.fao.org/3/x0490e/x0490e00.htm#Contents

Andrew D. Weiss. (2001). Topographic Position and Landforms Analysis. *ESRI Users Conference,SanDiego,CA*.

AppEEARS Team. (2022). *Application for Extracting and Exploring Analysis Ready Samples (AppEEARS).* (2.70). https://lpdaacsvc.cr.usgs.gov/appeears

Arnoldus, H. M. J. (1980). An approximation of the rainfall factor in the Universal Soil Loss Equation. *Assessment of Erosion, John Wiley and Sons Ltd*, 127–132.

Atkinson, P. M., & Massari, R. (1998). GENERALISED LINEAR MODELLING OF SUSCEPTIBILITY TO LANDSLIDING IN THE CENTRAL APENNINES, ITALY. *Computers & Geosciences*, *24*(4), 373–385.

Avdan, U., & Jovanovska, G. (2016). Algorithm for automated mapping of land surface temperature using LANDSAT 8 satellite data. *Journal of Sensors*, *2016*. https://doi.org/10.1155/2016/1480307

Ayalew, L., & Yamagishi, H. (2005). The application of GIS-based logistic regression for landslide susceptibility mapping in the Kakuda-Yahiko Mountains, Central Japan. *Geomorphology*, *65*(1–2), 15–31. https://doi.org/10.1016/J.GEOMORPH.2004.06.010

Bakhit, A., & Ibrahim, F. N. (1982). Geomorphological Aspects of the Process of Desertification in Western Sudan. In *Source: GeoJournal* (Vol. 6, Issue 1).

Basso, B., de Simone, L., Ferrara, A., Cammarano, D., Cafiero, G., Yeh, M. L., & Chou, T. Y. (2010). Analysis of contributing factors to desertification and mitigation measures in Basilicata region. *Italian Journal of Agronomy*, *5*(SUPPL. 3), 33–44. https://doi.org/10.4081/IJA.2010.S3.33

Benabbas, C. (2006). *Mio-Plio-Quaternary evolution of the continental basins of north-eastern Algeria : contribution of photogeology and morpho-structural analysis*. University of Mentouri, Constantine/Algeria.

Bivand, R., & Keitt, T. (2017). *Rgdal: Bindings for the "Geospatial" Data Abstraction Library* (1.2-16). https://r-forge.r-project.org/projects/rgdal/

Bivand, R., & Rundel, C. (2021). *Rgeos: Interface to Geometry Engine - Open Source ('GEOS')* (0.6-1). https://r-forge.r-project.org/projects/rgeos/

Borrelli, P., Panagos, P., Ballabio, C., Lugato, E., Weynants, M., & Montanarella, L. (2016). Towards a Pan-European Assessment of Land Susceptibility to Wind Erosion. *Land Degradation and Development*, *27*(4), 1093–1105. https://doi.org/10.1002/ldr.2318

Borrelli, P., Panagos, P., & Montanarella, L. (2015). New insights into the geography and modelling of wind erosion in the European agricultural land. Application of a spatially explicit indicator of land susceptibility to wind erosion. *Sustainability (Switzerland)*, *7*(7), 8823–8836. https://doi.org/10.3390/su7078823

Boudjemline, F., & Semar, A. (2018). Assessment and mapping of desertification sensitivity with MEDALUS model and GIS - Case study: Basin of Hodna, Algeria. *Journal of Water and Land Development*, *36*(1), 17–25. https://doi.org/10.2478/jwld-2018-0002

Bouhata, R., & Kalla, M. (2014). Mapping of environmental vulnerability of desertification by adaptation of the medalus method in the endoreic area of gadaine (eastern Algeria). *Geographia Technica*, *9*(2), 1–8.

Boureboune, L., & Benazzouz, M. T. (2009). *Aeolian Morphogenesis And Strategy Of Fight Against Desertification In Algeria (Hodna And Zibans Basin) BT - Desertification and Risk Analysis Using High and Medium Resolution Satellite Data* (A. Marini & M. Talbi (eds.); pp. 91–103). Springer Netherlands.

Brenning, A. (2005). Spatial prediction models for landslide hazards: Review, comparison and evaluation. *Natural Hazards and Earth System Science*, *5*(6), 853–862. https://doi.org/10.5194/nhess-5-853-2005

Carlson, T. N., & Ripley, D. A. (1997). On the relation between NDVI, fractional vegetation cover, and leaf area index. *Remote Sensing of Environment*, *62*(3), 241–252. https://doi.org/10.1016/S0034-4257(97)00104-1

Chepil, W. S., Siddoway, F. H., & Armbrust, D. V. (1962). Climatic factor for estimating wind erodibility of farm fields. *Journal of Soil and Water Conservation*.

CIESIN, C. for I. E. S. I. N. (2013). *Global Roads Open Access Data Set, Version 1 (gROADSv1)*. NASA Socioeconomic Data and Applications Center (SEDAC). https://doi.org/10.7927/H4VD6WCT

Conoscenti, C., Angileri, S., Cappadonia, C., Rotigliano, E., Agnesi, V., & Märker, M. (2014). Gully erosion susceptibility assessment by means of GIS-based logistic regression: A case of Sicily (Italy). *Geomorphology*, *204*, 399–411.

Croitoru, A. E., Piticar, A., Dragotă, C. S., & Burada, D. C. (2013). Recent changes in reference evapotranspiration in Romania. *Global and Planetary Change*, *111*, 127–136. https://doi.org/10.1016/j.gloplacha.2013.09.004

D.Nedjraoui and S. Bedrani. (2002). Desertification in the Algerian Steppe: Causes , impacts and actions in the fight. *Vertigo - La Revue Électronique En Sciences de l'environnement*, *8*(1), 1–15.

D'Odorico, P., Bhattachan, A., Davis, K. F., Ravi, S., & Runyan, C. W. (2013). Global desertification: Drivers and feedbacks. *Advances in Water Resources*, *51*, 326–344. https://doi.org/10.1016/j.advwatres.2012.01.013

Dai, F. C., & Lee, C. F. (2002). Landslide characteristics and slope instability modeling using GIS, Lantau Island, Hong Kong. *Geomorphology*, *42*, 213–228. www.elsevier.com/locate/geomorph

De Pina Tavares, J., Baptista, I., Ferreira, A. J. D., Amiotte-Suchet, P., Coelho, C., Gomes, S., Amoros, R., Dos Reis, E. A., Mendes, A. F., Costa, L., Bentub, J., & Varela, L. (2015). Assessment and mapping the sensitive areas to desertification in an insular Sahelian mountain region Case study of the Ribeira Seca Watershed, Santiago Island, Cabo Verde. *Catena*, *128*, 214–223. https://doi.org/10.1016/j.catena.2014.10.005

De Reu, J., Bourgeois, J., Bats, M., Zwertvaegher, A., Gelorini, V., De Smedt, P., Chu, W., Antrop, M., De Maeyer, P., Finke, P., Van Meirvenne, M., Verniers, J., & Crombé, P. (2013). Application of the topographic position index to heterogeneous landscapes. *Geomorphology*, *186*, 39–49. https://doi.org/10.1016/j.geomorph.2012.12.015

DESERTLINKS. (2004). *Desertification Indicator System for Mediterranean Europe*. https://esdac.jrc.ec.europa.eu/public_path/shared_folder/projects/DIS4ME/indicator_descriptions/drainage_density.htm

Didan, K. (2021). MODIS/Terra Vegetation Indices 16-Day L3 Global 250 m SIN Grid V061 [dataset]. *NASA EOSDIS Land Processes DAAC.[En Línea][Fecha de Consulta: 18 de Junio de 2021 En: Https://Doi. Org/10.5067/MODIS/MOD13Q1. 061*.

Djeddaoui, F., Chadli, M., & Gloaguen, R. (2017). Desertification Susceptibility Mapping Using Logistic Regression Analysis in the Djelfa Area, Algeria. *Remote Sensing 2017, Vol. 9, Page 1031*, *9*(10), 1031. https://doi.org/10.3390/RS9101031

Djoukbala, O., Hasbaia, M., Benselama, O., Hamouda, B., Djerbouai, S., Ferhati, A., Djoukbala, O., Hasbaia, Á. M., Benselama, Á. O., Djerbouai, Á. S., Ferhati, Á. A., & Hamouda Badji-Moukhtar, B. (2022). *Water Erosion and Sediment Transport in an Ungauged Semiarid Area: The Case of Hodna Basin in Algeria*. 439–454. https://doi.org/10.1007/978-981-16-2904-4_17

Esri. (2019). *ArcGIS Desktop: ArcMap 10.7.1*. Environmental Systems Research Institute.

Evans, I. S. (1972). General geomorphometry, derivatives of altitude, and descriptive statistics. In *Spatial Analysis in Geomorphology* (1st Editio, p. 74). Routledge.

Farr, T. G., Rosen, P. A., Caro, E., Crippen, R., Duren, R., Hensley, S., Kobrick, M., Paller, M., Rodriguez, E., Roth, L., Seal, D., Shaffer, S., Shimada, J., Umland, J., Werner, M., Oskin, M., Burbank, D., & Alsdorf, D. E. (2007). The shuttle radar topography mission. *Reviews of Geophysics*, *45*(2). https://doi.org/10.1029/2005RG000183

Fawcett, T. (2005). ROC graphs: Notes and practical considerations for researchers. *HP Laboratories*, 1–38. http://scholar.google.com/scholar?hl=en&btnG=Search&q=intitle:ROC+Graphs:+Notes+and+Practical+Considerations+for+Researchers#0

Feng, Q., Ma, H., Jiang, X., Wang, X., & Cao, S. (2015). What Has Caused Desertification in China? In *Scientific Reports* (Vol. 5, Issue 1). Nature Publishing Group. https://doi.org/10.1038/srep15998

Ferrara, A., Kosmas, C., Salvati, L., Padula, A., Mancino, G., & Nolè, A. (2020). Updating the MEDALUS-ESA Framework for Worldwide Land Degradation and Desertification Assessment. *Land Degradation and Development*, *31*(12), 1593–1607. https://doi.org/10.1002/ldr.3559

Fick, S. E., & Hijmans, R. J. (2017). WorldClim 2: new 1-km spatial resolution climate surfaces for global land areas. *International Journal of Climatology*, *37*(12), 4302–4315. https://doi.org/10.1002/joc.5086

Fryrear, D. W., Bilbro, J. D., Saleh, A., Schomberg, H., Stout, J. E., & Zobeck, T. M. (2000). RWEQ: Improved wind erosion technology. *Journal of Soil and Water Conservation*, *55*(2), 183–189.

Fryrear, D. W., Krammes, C. A., Williamson, D. L., & Zobeck, T. M. (1994). Computing the wind erodible fraction of soils. *Journal of Soil and Water Conservation*, *49*(2), 183–188.

Fryrear, D. W., Saleh, A., Bilbro, J. D., Schomberg, H. M., Stout, J. E., & Zobeck, T. M. (1998). Revised Wind Erosion Equation (RWEQ). *Technical Bulletin 1*.

Gad, A. (2020). *Qualitative and Quantitative Assessment of Land Degradation and Desertification in Egypt Based on Satellite Remote Sensing: Urbanization, Salinization and Wind Erosion* (pp. 443–497). https://doi.org/10.1007/978-3-030-39593-3_15

Gersie, S. P., Augustine, D. J., & Derner, J. D. (2019). Cattle Grazing Distribution in Shortgrass Steppe: Influences of Topography and Saline Soils. *Rangeland Ecology and Management*, *72*(4), 602–614. https://doi.org/10.1016/j.rama.2019.01.009

Ghebrezgabher, M. G., Yang, T., Yang, X., & Wang, C. (2019). Assessment of desertification in Eritrea: land degradation based on Landsat images. *Journal of Arid Land*, *11*(3), 319–331. https://doi.org/10.1007/s40333-019-0096-4

Ghosal, K., & Das Bhattacharya, S. (2020). A Review of RUSLE Model. *Journal of the Indian Society of Remote Sensing*, *48*(4), 689–707. https://doi.org/10.1007/s12524-019-01097-0

Gilbert, M., Nicolas, G., Cinardi, G., Van Boeckel, T. P., Vanwambeke, S. O., Wint, G. R. W., & Robinson, T. P. (2018). Global distribution data for cattle, buffaloes, horses, sheep, goats, pigs, chickens and ducks in 2010. *Scientific Data*, *5*, 1–11. https://doi.org/10.1038/sdata.2018.227

Glantz, M. H., & Orlovsky, N. S. (1983). Desertification: A review of the concept. *Desertification Control Bulletin*, *9*, 15–22.

Grecu, F. (2016). *Natural hazards and risks*. Editura Universitara. https://doi.org/10.5682/9786062803926

Grecu, F. (2018). *Dynamic pluvio-fluvial geomorphology.Theory and applications*. University Publishing House. https://doi.org/10.5682/9786062807276

Grecu, F., M, V., & S, C. (2017). Rainfall erosion and water erosion on the slopes of plateau in Romania. *“Climate, City and Environment”, Proceedings of the AIC Colloquium of Sfax*, 311–318.

Hadeel, A. S., Jabbar, M. T., & Chen, X. (2010). Application of remote sensing and GIS in the study of environmental sensitivity to desertification: A case study in Basrah Province, southern part of Iraq. *Applied Geomatics*, *2*(3), 101–112. https://doi.org/10.1007/s12518-010-0024-y

Han, J., Park, S., Kim, S., Son, S., Lee, S., & Kim, J. (2019). Performance of logistic regression and support vector machines for seismic vulnerability assessment and mapping: a case study of the 12 September 2016 ML5. 8 Gyeongju Earthquake, South Korea. *Sustainability*, *11*(24), 7038.

Harris, I., Jones, P. D., Osborn, T. J., & Lister, D. H. (2014). Updated high-resolution grids of monthly climatic observations - the CRU TS3.10 Dataset. *International Journal of Climatology*, *34*(3), 623–642. https://doi.org/10.1002/joc.3711

Harris, I., Osborn, T. J., Jones, P., & Lister, D. (2020). Version 4 of the CRU TS monthly high-resolution gridded multivariate climate dataset. *Scientific Data*, *7*(1). https://doi.org/10.1038/s41597-020-0453-3

Hijmans, R. J., & Etten, J. van. (2012). *Raster: Geographic analysis and modeling with raster data. R package version 2.0-12* (2.0-12). http://cran.r-project.org/package=raster

Ian D. Moore, & Gordon J. Burch. (1986). Physical Basis of the Length-slope Factor in the Universal Soil Loss Equation. *Soil Science Society of America*, *50*(5), 1294–1298.

J.Geist, H., & F.Lambin, E. (2004). Dynamic Causal Patterns of Desertification. *BioScience*, *54*(9), 817. https://doi.org/10.1641/0006-3568(2004)054[0817:dcpod]2.0.co;2

J.R. Williams. (1995). The EPIC model. *Computer Models of Watershed Hydrology, Water Resources Publications*, 909–1000.

Javed Mallick, Y. K., & B.D.Bharath. (2008). Estimation of land surface temperature over Delhi using Landsat-7 ETM+. *J. Ind. Geophys. Union*, *12*(3), 131–140. http://www.igu.in/12-3/5javed.pdf

Jones, H. G., & Vaughan, R. A. (2010). *Remote sensing of vegetation: principles, techniques, and applications*. Oxford university press.

Joseph F. Hair, William C. Black, Barry J. Babin, & Rolph E. Anderson. (2009). Multivariate Data Analysis (7th Edition). *Prentice Hall*.

Junek, W. N., Jones, W. L., & Woods, M. T. (2012). Use of logistic regression for forecasting short-term volcanic activity. *Algorithms*, *5*(3), 330–363.

K.G. Renard, K. Renard, GR Foster, G. Weesies, D McCool, D. Yoder, & G. Foster. (1997). *Predicting soil erosion by water: a guide to conservation planning with the revised universal soil loss equation (RUSLE)*.

Kaabeche, M. (1996). Les relations climat-végétation dans le bassin du Hodna (Algérie). *Acta Botanica Gallica*, *143*(1), 85–94. https://doi.org/10.1080/12538078.1996.10515321

Kairis, O., Karamanos, A., Voloudakis, D., Kapsomenakis, J., Aratzioglou, C., Zerefos, C., & Kosmas, C. (2022). Identifying Degraded and Sensitive to Desertification Agricultural Soils in Thessaly, Greece, under Simulated Future Climate Scenarios. *Land*, *11*(3). https://doi.org/10.3390/land11030395

Kairis, O., Kosmas, C., Karavitis, C., Ritsema, C., Salvati, L., Acikalin, S., Alcalá, M., Alfama, P., Atlhopheng, J., Barrera, J., Belgacem, A., Solé-Benet, A., Brito, J., Chaker, M., Chanda, R., Coelho, C., Darkoh, M., Diamantis, I., Ermolaeva, O., … Ziogas, A. (2014). Evaluation and Selection of Indicators for Land

Degradation and Desertification Monitoring: Types of Degradation, Causes, and Implications for Management. *Environmental Management*, *54*(5), 971–982. https://doi.org/10.1007/S00267-013-0110-0/TABLES/2

Kebiche, M. (1994). Le bassin versant du Hodna (Algérie): Ressources en eau et possibilités d'aménagement. *Travaux de l'Institut Géographique de Reims*, *85*(1), 25–34. https://doi.org/10.3406/tigr.1994.1298

Khan, A., Chatterjee, S., & Weng, Y. (2021). Characterizing thermal fields and evaluating UHI effects. *Urban Heat Island Modeling for Tropical Climates*, 37–67. https://doi.org/10.1016/B978-0-12-819669-4.00002-7

Khan, N. M., Rastoskuev, V. V, Shalina, E. V, & Sato, Y. (2001). *Mapping Salt-affected Soils Using Remote Sensing Indicators-A Simple Approach With the Use of GIS IDRISI*.

Kibblewhite, M., Rubio, J., Kosmas, C., Jones, R., Arrouays, D., Huber, S., & Verheijen, F. (2007). ENVASSO-Environmental assessment of soil for monitoring desertification in Europe. *8.Conference of the Parties of the United Nations Convention to Combat Desertificatio*, 62.

Kosmas, C., Kirkby, M., & Geeson, N. (1999). Manual on Key Indicators of Desertification and Mapping Environmentally Sensitive Areas to Desertification. *European Commission, Energy, Environment and Sustainable Development*, *EUR 18882*.

Kosmas, C., Tsara, M., & Karavitis, C. A. (2003). Identification of indicators for desertification. *Annals of Arid Zone*, *42*(3), 393–416. https://www.researchgate.net/publication/279767083

Kosmas, C., Tsara, M., Moustakas, N., Kosma, D., & Yassoglou, N. (2006). Environmentally Sensitive Areas and Indicators of Desertification. In *Desertification in the Mediterranean Region. A Security Issue*. https://doi.org/10.1007/1-4020-3760-0_25

Lal, R. (2001). Soil degradation by erosion. *Land Degradation and Development*, *12*(6), 519–539. https://doi.org/10.1002/ldr.472

Lamchin, M., Lee, J. Y., Lee, W. K., Lee, E. J., Kim, M., Lim, C. H., Choi, H. A., & Kim, S. R. (2016). Assessment of land cover change and desertification using remote sensing technology in a local region of Mongolia. *Advances in Space Research*, *57*(1), 64–77. https://doi.org/10.1016/J.ASR.2015.10.006

Lamqadem, A. A., Saber, H., & Pradhan, B. (2018). Quantitative assessment of desertification in an arid oasis using remote sensing data and spectral index techniques. *Remote Sensing*, *10*(12). https://doi.org/10.3390/rs10121862

Li, Z. L., Tang, B. H., Wu, H., Ren, H., Yan, G., Wan, Z., Trigo, I. F., & Sobrino, J. A. (2013). Satellite-derived land surface temperature: Current status and perspectives. *Remote Sensing of Environment*, *131*, 14–37. https://doi.org/10.1016/j.rse.2012.12.008

Longley, P., Smith, M. J. De, & F.Goodchild, M. (2007). *Geospatial Analysis A Comprehensive Guide to Principles, Techniques and Software Tools* (Matador (ed.)).

López-Bermúdez, F. (1990). Soil erosion by water on the desertification of a semi-arid Mediterranean fluvial basin: the Segura basin, Spain. *Agriculture, Ecosystems and Environment*, *33*(2), 129–145. https://doi.org/10.1016/0167-8809(90)90238-9

Louviere, J. J., Hensher, D. A., & Swait, J. D. (2000). *Stated choice methods: analysis and applications*. Cambridge university press.

Mathew, J., Jha, V. K., & Rawat, G. S. (2009). Landslide susceptibility zonation mapping and its validation in part of Garhwal Lesser Himalaya, India, using binary logistic regression analysis and receiver operating characteristic curve method. *Landslides*, *6*(1), 17–26. https://doi.org/10.1007/s10346-008-0138-z

Mihi, A., Ghazela, R., & wissal, D. (2022). Mapping potential desertification-prone areas in North-Eastern Algeria using logistic regression model, GIS, and remote sensing techniques. *Environmental Earth Sciences*, *81*(15), 1–14. https://doi.org/10.1007/s12665-022-10513-7

Mind'je, R., Li, L., Amanambu, A. C., Nahayo, L., Nsengiyumva, J. B., Gasirabo, A., & Mindje, M. (2019). Flood susceptibility modeling and hazard perception in Rwanda. *International Journal of Disaster Risk Reduction*, *38*, 101211.

Mirzabaev, A., J. Wu, J. Evans, F. García-Oliva, I.A.G. Hussein, M.H. Iqbal, J. Kimutai, T. Knowles, F. Meza, D. Nedjraoui, F. Tena, M. Türkeş, R.J. Vázquez, & M. Weltz. (2019). *Climate Change and Land: an IPCC special report on climate change, desertification, land degradation, sustainable land management, food security, and greenhouse gas fluxes in terrestrial ecosystems*. Ali Mohammed.

Mirzabaev, A., Stringer, L. C., Benjaminsen, T. A., Gonzalez, P., Harris, R., Jafari, M., Stevens, N., Tirado, C. M., & Zakieldeen, S. (2022). Cross-chapter paper 3: deserts, semi-arid areas and desertification. *Climate Change*, 2195–2231. https://doi.org/10.1017/9781009325844.020

Musy, A. (2005). *Cours "Hydrologie générale."* https://echo2.epfl.ch/e-drologie/

Novák, V. (2011). Evapotranspiration. In J. Gliński, J. Horabik, & J. Lipiec (Eds.), *Encyclopedia of Agrophysics* (pp. 280–283). Springer Netherlands. https://doi.org/10.1007/978-90-481-3585-1_55

O'Brien, R. M. (2007). A caution regarding rules of thumb for variance inflation factors. *Quality and Quantity*, *41*(5), 673–690. https://doi.org/10.1007/s11135-006-9018-6

Oldeman, L. R. (1991). Global Extent of Soil Degradation. In *ISRIC Bi-Annual Report*.

Parry, M. L. (2007). *Climate change 2007-impacts, adaptation and vulnerability: Working group II* *contribution to the fourth assessment report of the IPCC* (Vol. 4). Cambridge University Press.

R Core Team. (2016). *R:A language and Environment for Statistical Computing*. https://www.r-project.org/

Román, M. O., Wang, Z., Sun, Q., Kalb, V., Miller, S. D., Molthan, A., Schultz, L., Bell, J., Stokes, E. C., Pandey, B., Seto, K. C., Hall, D., Oda, T., Wolfe, R. E., Lin, G., Golpayegani, N., Devadiga, S., Davidson, C., Sarkar, S., … Masuoka, E. J. (2018). NASA's Black Marble nighttime lights product suite. *Remote Sensing of Environment*, *210*(March), 113–143. https://doi.org/10.1016/j.rse.2018.03.017

RStudio Team. (2015). *RStudio: Integrated Development Environment for R. Boston, MA* (2022.02.4). http://www.rstudio.com/

Rubio, J. L., & Bochet, E. (1998). *Desertification indicators as diagnosis criteria for desertification risk assessment in Europe*.

Running, S., Mu, Q., M., Z., & Moreno, A. (2021). *MODIS/Terra Net Evapotranspiration Gap-Filled 8-Day L4 Global 500m SIN Grid V061. NASA EOSDIS Land Processes DAAC*. https://doi.org/https://doi.org/10.5067/MODIS/MOD16A2GF.061

Saifi, M., Boulghobra, N., & Fattoum, L. (2014). The green Dam in Algeria as a Tool to Combat Desertification., vol. 3 (2015). *Davos: Global Risk Forum) MEED Insight. Middle East Rail and Metro Projects Report*, *January 2015*, 1–4.

Salih, A., Hassaballa, A. A., & Ganawa, E. (2021). Mapping desertification degree and assessing its severity in Al-Ahsa Oasis, Saudi Arabia, using remote sensing-based indicators. *Arabian Journal of Geosciences*, *14*(3). https://doi.org/10.1007/s12517-021-06523-7

Sanderson, E. W., Jaiteh, M., Levy, M. A., Redford, K. H., Wannebo, A. V., & Woolmer, G. (2002). The Human Footprint and the Last of the Wild. *BioScience*, *52*(10), 891–904. https://doi.org/https://doi.org/10.1641/0006-3568(2002)052[0891:THFATL]2.0.CO;2

Shan, N., Shi, Z., Yang, X., Zhang, X., Guo, H., Zhang, B., & Zhang, Z. (2016). Trends in potential evapotranspiration from 1960 to 2013 for a desertification-prone region of China. *International Journal of Climatology*, *36*(10), 3434–3445. https://doi.org/10.1002/joc.4566

Shao Y; Leslie, L. (1997). Wind erosion prediction over the Australian continent. *J. of Geophysical Research*, *102*(97), 91–105.

Shao, Y. (2008). Physics and Modelling of Wind Erosion (Atmospheric and Oceanographic Sciences Library, 37). *Springer*.

Sing, T., Sander, O., Beerenwinkel, N., Lengauer, T., & Unterthiner, T. (2015). *ROCR: visualizing classifier performance in R* (1.0-11). Bioinformatics, 21(20).

Skidmore, E. L. (1986). Wind erosion climatic erosivity. *Climatic Change*, *9*(1–2), 195–208. https://doi.org/10.1007/BF00140536

Skidmore, E. L. (1994). Wind Erosion. In Routledge (Ed.), *Soil Erosion Research Methods* (2nd Editio, p. 352). Soil and Water Conservation Society (U. S.). https://doi.org/https://doi.org/10.1201/9780203739358

Smith, T. J., & Mckenna, C. M. (2013). *A Comparison of Logistic Regression Pseudo R 2 Indices* (Vol. 39, Issue 2).

Sobrino, J. A., Jiménez-Muñoz, J. C., & Paolini, L. (2004). Land surface temperature retrieval from LANDSAT TM 5. *Remote Sensing of Environment*, *90*(4), 434–440. https://doi.org/10.1016/j.rse.2004.02.003

Sternberg, T., Tsolmon, R., Middleton, N., & Thomas, D. (2011). Tracking desertification on the Mongolian steppe through NDVI and field-survey data. *International Journal of Digital Earth*, *4*(1), 50–64. https://doi.org/10.1080/17538940903506006

Tahar, M., & Boureboune, L. (2009). *Anthropic Actions And Desertification In Algeria BT - Desertification and Risk Analysis Using High and Medium Resolution Satellite Data* (A. Marini & M. Talbi (eds.); pp. 3–18). Springer Netherlands.

Tai, X., Epstein, H. E., & Li, B. (2020). Elevation and climate effects on vegetation greenness in an arid mountain-basin system of Central Asia. *Remote Sensing*, *12*(10). https://doi.org/10.3390/rs12101665

Verstraete, M. M., & Schwartz, S. A. (1991). Desertification and global change. *Vegetatio*, *91*(1–2), 3–13. https://doi.org/10.1007/BF00036043

Wang, X., Chen, F., Hasi, E., & Li, J. (2008). Desertification in China: An assessment. *Earth-Science Reviews*, *88*(3–4), 188–206. https://doi.org/10.1016/j.earscirev.2008.02.001

Wehrhan, M., & Sommer, M. (2021). A parsimonious approach to estimate soil organic carbon applying unmanned aerial system (Uas) multispectral imagery and the topographic position index in a heterogeneous soil landscape. *Remote Sensing*, *13*(18). https://doi.org/10.3390/rs13183557

Wever, N. (2012). Quantifying trends in surface roughness and the effect on surface wind speed observations. *Journal of Geophysical Research Atmospheres*, *117*(11), 1–14. https://doi.org/10.1029/2011JD017118

Wischmeier, W. H., & Smith, D. D. (1978). *Predicting Rainfall Erosion Losses: A Guide to Conservation Planning. The USDA Agricultural Handbook No. 537*.

YAKHLEFOUNE, M., BENABBAS, C., GRECU, F., BELKENDIL, A., & KHARCHI, T.-E. (2023). Flood risk modelling using HEC-RAS and GIS in the semi-urban watershed of Oued Ziad (Constantine, North-Eastern Algeria). *Forum Geografic*, *22*(1).

Yong-Zhong, S., Yu-Lin, L., Jian-Yuan, C., & Wen-Zhi, Z. (2005). Influences of continuous grazing and livestock exclusion on soil properties in a degraded sandy grassland, Inner Mongolia, northern China. *Catena*, *59*(3), 267–278. https://doi.org/10.1016/j.catena.2004.09.001

Yu, X., Lei, J., & Gao, X. (2022). An over review of desertification in Xinjiang, Northwest China. *Journal of Arid Land*, *14*(11), 1181–1195. https://doi.org/10.1007/s40333-022-0077-x

Zanaga, D., Van De Kerchove, R., De Keersmaecker, W., Souverijns, N., Brockmann, C., Quast, R., Wevers, J., Grosu, A., Paccini, A., Vergnaud, S., Cartus, O., Santoro, M., Fritz, S., Georgieva, I., Lesiv, M., Carter, S., Herold, M., Li, L., Tsendbazar, N.-E., … Arino, O. (2021). *ESA WorldCover 10 m 2020 v100*. https://doi.org/10.5281/ZENODO.5571936

Zobeck, T. M. (1991). Soil properties affecting wind erosion. *Journal of Soil and Water Conservation*, *46*(2), 112–118.

Zou, X., Zhang, Z., Zhou, Z., Qiu, Q., & Luo, J. (2021). Landscape-scale spatial variability of soil organic carbon content in a temperate grassland: Insights into the role of wind erosion. *Catena*, *207*(June), 105635. https://doi.org/10.1016/j.catena.2021.105635